

Modelling constraints on the emission inventory and on vertical diffusion for CO and SO₂ in the Mexico City Metropolitan Area using Solar FTIR and zenith sky UV spectroscopy

B. de Foy¹, W. Lei², M. Zavala², R. Volkamer³, J. Samuelsson⁴, J. Mellqvist⁴, B. Galle⁴, A.-P. Martínez⁵, M. Grutter⁶, and L. T. Molina^{1,2}

¹Molina Center for Energy and the Environment, CA, USA

²Department of Earth, Atmospheric and Planetary Sciences, Massachusetts Institute of Technology, USA

³Department of Chemistry and Biochemistry, University of California, San Diego, USA

⁴Department of Radio and Space Science, Chalmers University of Technology, Gothenburg, Sweden

⁵General Direction of the National Center for Environmental Research and Training (CENICA), National Institute of Ecology (INE), Mexico

⁶Centro de Ciencias de la Atmósfera, Universidad Nacional Autónoma de México, México

Received: 19 June 2006 – Accepted: 20 June 2006 – Published: 11 July 2006

Correspondence to: B. de Foy (bdefoy@mce2.org)

Sources and
transport of CO and
SO₂ in the MCMA

B. de Foy et al.

Title Page

Abstract

Introduction

Conclusions

References

Tables

Figures

◀

▶

◀

▶

Back

Close

Full Screen / Esc

Printer-friendly Version

Interactive Discussion

Abstract

Emissions of air pollutants in and around urban areas lead to negative health impacts on the population. To estimate these impacts, it is important to know the sources and transport mechanisms of the pollutants accurately. Mexico City has a large urban fleet in a topographically constrained basin leading to high levels of carbon monoxide (CO). Large point sources of sulfur dioxide (SO₂) surrounding the basin lead to episodes with high concentrations. An Eulerian grid model (CAMx) and a particle trajectory model (FLEXPART) are used to evaluate the estimates of CO and SO₂ in the current emission inventory using mesoscale meteorological simulations from MM5. Vertical column measurements of CO are used to constrain the total amount of emitted CO in the model and to identify the most appropriate vertical diffusion scheme. Zenith sky UV spectroscopy is used to estimate the emissions of SO₂ from a large power plant and the Popocatepetl volcano. Results suggest that the models are able to identify correctly large point sources and that both the power plant and the volcano impact the MCMA. Modelled concentrations of CO based on the current emission inventory match observations suggesting that the current total emissions estimate is correct. Possible adjustments to the spatial and temporal distribution can be inferred from model results. Accurate source and dispersion modelling provides feedback for development of the emission inventory, verification of transport processes in air quality models and guidance for policy decisions.

1 Introduction

Detailed and accurate emission inventories are a cornerstone of effective air quality management programs. Public policy choices can be evaluated with air quality models based on actual emissions and alternative scenarios in combination with accurate meteorological simulations. This paper makes use of novel measurement techniques to evaluate the carbon monoxide (CO) inventory for the Mexico City Metropolitan Area

Sources and transport of CO and SO₂ in the MCMA

B. de Foy et al.

Title Page

Abstract

Introduction

Conclusions

References

Tables

Figures

⏪

⏩

◀

▶

Back

Close

Full Screen / Esc

Printer-friendly Version

Interactive Discussion

(MCMA) and to evaluate the potential impacts of large point sources of sulfur dioxide (SO₂). Even though vertical diffusion has a large impact on pollutant transport, it can be overlooked as a source of uncertainty. Pollution observations and simulations are further used to evaluate alternative vertical diffusion schemes.

5 1.1 Mexico City Metropolitan Area

Megacities are home to a growing number of people and can suffer from high levels of air pollution (Molina and Molina, 2004; Molina et al., 2004). The MCMA is a megacity of around 20 million people living in a basin 100 km diameter. The basin is surrounded by high mountains on the west, south and east and is located at high elevation, leading to intense solar radiation and high ozone levels most of the year. There has been extensive scientific study of the air quality in the MCMA, as reviewed in Molina and Molina (2002).

Nickerson et al. (1992) carried out aircraft profiles of ozone, SO₂ and particulate matter (PM) above Mexico City in 1991, highlighting the importance of combustion sources for the basin air pollution. Williams et al. (1995) modelled air dispersion for the same episodes looking at the transport of contaminants towards the southwest of the basin and emphasizing the need for improved accuracy of the emission inventory. Elliott et al. (1997) analyse the importance of liquefied petroleum gas (LPG) components in the urban air chemistry. By estimating CO life times of approximately 2 days in the basin, estimates are made of the LPG venting to the regional environment.

Fast and Zhong (1998) developed a wind circulation model for the basin from data obtained during the IMADA campaign of 1997. This emphasized the importance of vertical mixing and mountain winds in the transport of the urban plume first towards the south and then back over the city to the north. Similar patterns are described in Jazcilevich et al. (2003) with evidence of direct convective transport from layers aloft to the surface. West et al. (2004) modelled the photochemistry in the basin during the IMADA campaign, suggesting that the emission inventory for CO be scaled by a factor of 2 and that of volatile organic compounds (VOCs) by a factor of 3.

Sources and transport of CO and SO₂ in the MCMA

B. de Foy et al.

Title Page

Abstract

Introduction

Conclusions

References

Tables

Figures

◀

▶

◀

▶

Back

Close

Full Screen / Esc

Printer-friendly Version

Interactive Discussion

MCMA-2003 was a major field campaign that took place in April 2003. [De Foy et al. \(2005\)](#) classified the meteorological conditions into 3 episode types which were subsequently used to analyse the transport and basin venting ([de Foy et al., 2006c](#)). In particular, this found short residence times in the basin and little carry-over from day to day.

1.2 Emission inventory

Emission inventories can be derived using either the “top-down” method, where total fuel and energy consumption are used for a whole region to determine surface emissions or the “bottom-up” method, where estimates of vehicle miles travelled and residential, industrial and commercial energy use patterns are considered. The 2002 official emission inventory for the MCMA used in this study was derived by the bottom-up method by the Comisión Ambiental Metropolitana (CAM) of the Mexican Federal District government ([Comisión Ambiental Metropolitana, 2004](#)). This contains annual totals for the criteria pollutants which need to be temporally and spatially distributed as well as speciated for VOCs ([West et al., 2004](#)).

[Schifter et al. \(2005\)](#) develop a top-down estimate of vehicular emissions by combining fuel use statistics with emission factors obtained from in-situ remote sensing experiments. This suggests that there has been a reduction in MCMA emissions and that, if anything, the official inventory may overestimate CO emissions. [Jiang et al. \(2005\)](#) obtain emission factors for the MCMA vehicle fleet by analysing data from the Aerodyne mobile laboratory ([Kolb et al., 2004](#)) for CO, black carbon, polycyclic aromatic hydrocarbons and other pollutants. For CO, a similar conclusion to [Schifter et al. \(2005\)](#) is drawn, that official inventory estimates are high but in general agreement. [Zavala et al. \(2006\)](#) analyse chase and fleet average mode data in detail, determining emission factors from individual vehicle plumes and obtaining emission estimates for individual vehicle types. This provides valuable information on NO_x, aldehydes, ammonia and certain VOC's which will be used to further refine the emission inventory and guide policy work.

Sources and transport of CO and SO₂ in the MCMA

B. de Foy et al.

Title Page

Abstract

Introduction

Conclusions

References

Tables

Figures

◀

▶

◀

▶

Back

Close

Full Screen / Esc

Printer-friendly Version

Interactive Discussion

On a more regional scale, [Kuhns et al. \(2005\)](#) report on the development of an emission inventory for the northern part of Mexico as part of the BRAVO study. This includes the MCMA inventory but not the surrounding region. [Olivier and Berdowski \(2001\)](#) develop the EDGAR global emission inventory at a 1 degree resolution. For Mexico however, the MCMA is about ten times larger than anthropogenic sources outside of the basin. This means that within the accuracy of the present modelling work, regional emissions can be represented through appropriate settings of the boundary conditions.

The BRAVO emission inventory also includes estimates of SO₂ emissions from the Popocatepetl volcano and the Tula industrial complex, two large point sources shown in Fig. 1. The Tula source consists of both a power plant and a refinery. The Popocatepetl volcano is an active volcano forming the south-eastern edge of the MCMA basin. It has been under continuous monitoring by the Centro Nacional de Prevención de Desastres (CENAPRED). [Kuhns et al. \(2005\)](#) report SO₂ emission estimates made with a correlation spectrometer (COSPEC) as high as 50 000 tons/day (metric) but more typically around 3000 to 5000 tons/day. [Galindo et al. \(1998\)](#) analyse the gas and particle emissions during the eruptions of December 1994 to January 1995. They report a baseline SO₂ emission rate of 1000 tons/day rising up to 5000 tons/day during eruptions. [Delgado-Granados et al. \(2001\)](#) further analyse COSPEC data to distinguish between pre-eruptive emissions of 2000 to 3000 tons/day and effusive-explosive periods with emissions up to 13 000 tons/day. They therefore classify the volcano as a high-emission rate, passively degassing eruptive volcano. This means that high SO₂ emissions are present in the absence of any visible ash plume. [Wright et al. \(2002\)](#) make use of GOES satellite thermal imagery to identify explosions, exhalations and cycles of dome growth of the volcano, which can be indicative of increased SO₂ emissions. [Matiella et al. \(2006\)](#)¹ use MODIS data to quantify the size of ash and SO₂

¹Matiella, M. A., Watson, I. M., Delgado-Granados, H., Rose, W. I., and Cardenas-Gonzalez, L.: Volcanic emissions from Popocatepetl volcano, Mexico, quantified using Moderate Resolution Imaging Spectroradiometer infrared data, *J. Volcanol. Geotherm. Res.*, in review, 2006.

Sources and transport of CO and SO₂ in the MCMA

B. de Foy et al.

Title Page

Abstract

Introduction

Conclusions

References

Tables

Figures

◀

▶

◀

▶

Back

Close

Full Screen / Esc

Printer-friendly Version

Interactive Discussion

clouds. SO₂ emission rates were found in broad agreement with COSPEC values of 5000 to 32 000 tons/day.

Regional export of sulfate aerosols was simulated by [Barth and Church \(1999\)](#) with a global model along with black carbon transport and oxidation. Mexico City was found to contribute approximately 1% to the global sulfate burden. [Marquez et al. \(2005\)](#) measured air quality 250 km east of the MCMA near a mountain top to further evaluate the effects of urban emissions on the regional environment. Volcanic degassing of SO₂ was not considered as a possible additional source however ([Pyle and Mather, 2005](#)). [Raga et al. \(1999\)](#) had previously analysed SO₂, CO and aerosol measurements in the MCMA and suggested that increased sulfate aerosol production in the city could be due to volcanic emissions. [Jimenez et al. \(2004\)](#) report on a field study carried out between Popocatepetl and Puebla (to the east). Clear evidence was found of volcanic influence at the surface for 6 out of 17 days sampled.

1.3 Measurements

Column measurements of CO can be used in conjunction with dispersion models to constrain emission inventories. For example, [Yurganov et al. \(2004\)](#) obtain CO columns from Fourier Transform Infrared (FTIR) spectrometers. A box model and the 3-D global GEOS-CHEM model ([Bey et al., 2001](#)) are used to evaluate the emissions from boreal wild fires in August 1998. [Yurganov et al. \(2005\)](#) extend the analysis to 2002 and 2003. Strong correlations are found between estimates from surface measurements and those from MOPITT CO columns.

Remote sensing of SO₂ can be used to estimate emission rates. Whereas CO sources are spread out and CO plumes broad, SO₂ sources are more likely to be large point sources with individual well-defined plumes. [Galle et al. \(2003\)](#) develop a miniaturised ultraviolet spectrometer to evaluate volcanic emissions. The “Mini-DOAS” is used to quantify emissions from 2 volcanoes and is compared with measurements from COSPEC. [Elias et al. \(2006\)](#) report further validation against COSPEC with agreement between the different systems within 10%. [McGonigle et al. \(2004\)](#) use the same

Sources and transport of CO and SO₂ in the MCMA

B. de Foy et al.

Title Page

Abstract

Introduction

Conclusions

References

Tables

Figures

◀

▶

◀

▶

Back

Close

Full Screen / Esc

Printer-friendly Version

Interactive Discussion

technique for estimating power plant emissions of both SO₂ and NO₂. Emission rates of 5.2 kg/s of SO₂ were remarkably close to in-stack monitor values of 5.3 kg/s, suggesting that this method provides an accurate, low-cost, easily deployable means of estimating and validating large point sources in emission inventories.

5 1.4 Source identification

[Blanchard \(1999\)](#) reviews different methods for estimating the impacts of emission sources on air pollutant levels. These can be separated into data analysis methods and model-based methods. The latter includes forward and backward trajectory analyses as well as Eulerian dispersion models. [Hopke \(2003\)](#) reviews further developments of receptor models and back trajectory analyses. “Residence Time Analysis” and “Potential Source Contribution Function” are described and compared using case studies in the northeast of the U.S.

“Residence Time Analysis” was introduced by [Ashbaugh et al. \(1985\)](#). It is a 2-D gridded field that represents the probability that a randomly selected air parcel is to be found in a grid cell relative to the total time interval of the trajectory. Dividing the probability of a “dirty” air parcel being in a grid cell with the probability of any air parcel passing through that cell, one obtains the “Potential Source Contribution Function”. This normalised field will have high values over regions of high emissions. The method was used to show that the dominant source of sulfur in the Grand Canyon national park was from southern California.

[Sirois and Bottenheim \(1995\)](#) define “Probability of Residence” by applying the Residence Time Analysis of [Ashbaugh et al. \(1985\)](#) to the trajectories associated with the highest and lowest 10% of air pollutant concentrations. A cluster analysis was then performed on all backward trajectories at the receptor site. Analysis of the pollution levels associated with each cluster showed agreement with the “Probability of Residence” method while providing additional information about air mass movements. [Vasconcelos et al. \(1996a\)](#) apply the method of [Ashbaugh et al. \(1985\)](#) to field campaign data in the Grand Canyon, again identifying southern California as the main source region.

Sources and transport of CO and SO₂ in the MCMA

B. de Foy et al.

Title Page

Abstract

Introduction

Conclusions

References

Tables

Figures

◀

▶

◀

▶

Back

Close

Full Screen / Esc

Printer-friendly Version

Interactive Discussion

Sources and transport of CO and SO₂ in the MCMAB. de Foy et al.

Title Page

Abstract

Introduction

Conclusions

References

Tables

Figures

◀

▶

◀

▶

Back

Close

Full Screen / Esc

Printer-friendly Version

Interactive Discussion

The spatial resolution of their results is analysed in [Vasconcelos et al. \(1996b\)](#). This suggested that the method has good resolution in source direction but significantly less in radial distance from the receptor site. Long trajectories (5 days in this case) have higher uncertainties, but short trajectories (3 days) can miss distant sources and suggest spurious source regions near the receptor.

[Stohl \(1998\)](#) reviews the applications and accuracy of trajectories. “Concentration Fields” are described as Residence Time Analysis multiplied by pollutant concentrations at the receptor site for each measurement time ([Seibert et al., 1994](#)). [Lupu and Maenhaut \(2002\)](#) show that the Potential Source Contribution Function and Concentration Field methods are in agreement over the identification of European emissions based on measurements at different peripheral sites. The bootstrap technique is used to estimate the statistical significance of potential sources, and known emission sources are shown to be correctly identified.

“Redistributed Concentration Fields” ([Stohl, 1996](#)) were shown to improve the spatial resolution of anthropogenic emissions in western Europe ([Wotawa and Kroger, 1999](#)) and were used to to analyse emissions of forest fires in Canada ([Wotawa and Trainer, 2000](#)). This method was applied to multiple measurement sites for particle sources in rural New York ([Zhou et al., 2004](#)). The emission inventory was correctly identified although some unrealistic estimations could be introduced. “Quantitative Transport Bias Analysis”, an alternative method, was shown to yield similar results.

[Begum et al. \(2005\)](#) evaluate the Potential Source Contribution Function for forest fires. By looking at different pollutants, the method is able to distinguish between biomass burning and urban sources and is found to have a good spatial resolution. [Issartel \(2003\)](#) further explores the limitations of the Potential Source Contribution Function. “Illumination” is developed to quantify how well a receptor site is able to see a potential source region, and how much information can be obtained given the data available.

When extensive measurements are present, such as speciated aerosol data, local sources can be identified by foregoing trajectories and using surface wind measure-

ments at the receptor site (Lee et al., 2006). Sanchez-Ccoylo et al. (2006) use clusters of trajectories to look at pollution sources in and around São Paulo based on measurements of ozone, CO and particulate matter.

Use of single trajectories does not account for the spread in possible source directions due to vertical and horizontal mixing. Jiang et al. (2003) calculate retro-plumes by running a dispersion model, CALPUFF, in reverse mode. This yields the equivalent of Concentration Fields that account for all the processes parameterised in CALPUFF, including diffusion and deposition. By replacing single trajectory analyses with a Lagrangian particle dispersion model, Stohl et al. (2002) account for both physical dispersion and numerical uncertainty in the trajectory locations.

1.5 Vertical diffusion

As the resolution of meteorological models increases both in the horizontal and in the vertical, the parameterisation of the surface energy budget and that of the vertical mixing become more important in terms of simulation accuracy (Zhong and Fast, 2003). Nevertheless, Berg and Zhong (2005) found that despite the different boundary layer schemes in MM5 and the different levels of mixing they simulate, there is little gain in the overall accuracy of the forecasts due to their increased complexity.

Validating or verifying vertical diffusion coefficients is difficult because the numerical representation does not account for the complexity of the physical process and because the diffusion coefficients cannot be measured directly. O'Brien (1970) proposed a simple parameterisation scheme used in many air quality models. Lee and Larsen (1997) applied this model to reproduce vertical profiles of ^{222}Rn in the lower atmosphere. Comparisons with observations suggested values of vertical mixing above the boundary layer. Olivie et al. (2004) carry out a similar analysis, using ^{222}Rn concentrations to evaluate different schemes.

For air quality models, the vertical diffusion has a direct impact on simulated surface concentrations. Nowacki et al. (1996) found excessive vertical mixing in the day time unstable boundary layer leading to errors in surface concentrations. Improvements

Sources and transport of CO and SO₂ in the MCMA

B. de Foy et al.

Title Page

Abstract

Introduction

Conclusions

References

Tables

Figures

◀

▶

◀

▶

Back

Close

Full Screen / Esc

Printer-friendly Version

Interactive Discussion

in the specification of the vertical diffusion coefficients were suggested but evaluation was limited due to the lack of measurements of the vertical concentration profiles. [Biswas and Rao \(2001\)](#) report substantial differences between different models adding to uncertainties in ozone simulations and [Roelofs et al. \(2003\)](#) suggest that coarse vertical resolution may lead to excessive diffusion.

[Brandt et al. \(1998\)](#) analysed different vertical diffusion schemes and found that the simplest scheme of high vertical diffusion yielded the best results, suggesting that non-local diffusion is an important factor. [Ulke and Andrade \(2001\)](#) propose a new parameterisation which yields higher surface concentrations in the CIT model. They also highlight the problem of validating emissions inventories with surface data but no vertical profiles. [Perez-Roa et al. \(2006\)](#) use artificial neural networks to develop site-specific optimal estimates of vertical diffusion coefficients. They show improved surface concentrations of CO and particulate matter using the CAMx model, as well as possible adjustments to the emission inventory.

1.6 Outline

This paper makes use of Concentration Fields from backward trajectories and forward Eulerian dispersion modelling to analyse the emission inventory for CO and SO₂. Column measurements of CO are used as a constraint on the vertical diffusion scheme. SO₂ emission fluxes are estimated from large point sources so as to simulate their impact on the MCMA. Section 2 describes the models used and Sect. 3 the observations. The analysis of the emission inventory is split by pollutant: Sect. 4 looks at CO and Sect. 5 looks at SO₂. Each section is split into a first part using backward trajectories, a second part using Eulerian modelling and a discussion section.

Sources and transport of CO and SO₂ in the MCMA

B. de Foy et al.

Title Page

Abstract

Introduction

Conclusions

References

Tables

Figures

◀

▶

◀

▶

Back

Close

Full Screen / Esc

Printer-friendly Version

Interactive Discussion

2 Model description

The Pennsylvania State University/National Center for Atmospheric Research Mesoscale Model (MM5, [Grell et al., 1995](#)) version 3.7.2 was used to generate the wind fields as described in [de Foy et al. \(2006b\)](#). This uses three nested grids with one-way nesting at resolutions of 36, 12 and 3 km, with 40×50, 55×64 and 61×61 grid cells for domains 1, 2 and 3, respectively, and are the same simulations used in [de Foy et al. \(2006a\)](#). The initial and boundary conditions were taken from the Global Forecast System (GFS) at a 3-h resolution. High resolution satellite remote sensing is used to initialise the land surface parameters for the NOAH land surface model, as described in [de Foy et al. \(2006b\)](#).

The emission inventory used for CO and SO₂ is based on [West et al. \(2004\)](#) with updated totals from [Comisión Ambiental Metropolitana \(2004\)](#). The spatial pattern of the CO area sources is shown in Fig. 2a, and the point sources in Fig. 2c. The SO₂ emissions are shown in Figs. 2b and d. The temporal profile of both CO and SO₂ is shown in Fig. 3. This shows that the point sources are negligible for CO and small for SO₂, although including the Tula industrial complex and Popocatépetl volcano would change this picture. There is a clear peak at the morning rush hour, sustained traffic throughout the day and reduced emissions at night.

Stochastic particle trajectories are calculated using FLEXPART ([Stohl et al., 2005](#)), as described in [de Foy et al. \(2006c\)](#). Backward trajectories are calculated for specific fixed sites. For these cases, 100 particles per hour are released between 0 and 50 m above ground and are traced back for 48 h. Forward trajectories are calculated with the CO spatial and temporal distribution described above to provide simulated CO fields.

Residence Time Analysis was carried out using the particle simulations following [Ashbaugh et al. \(1985\)](#). For a one hour release, all particle positions at every hour of the simulation are stored. A surface grid is applied over the simulation domain, and all particle positions in each grid cell are totalled for the entire simulation. This gives “Residence Times”, the grid corresponds to a time exposure photograph of the

Sources and transport of CO and SO₂ in the MCMA

B. de Foy et al.

Title Page

Abstract

Introduction

Conclusions

References

Tables

Figures

◀

▶

◀

▶

Back

Close

Full Screen / Esc

Printer-friendly Version

Interactive Discussion

particle tracks, with values equivalent to the length of time spent in each cell by particles emitted.

The Residence Times can be summed for hourly releases during the whole campaign to identify preferred transport directions. In order to identify possible source regions, Concentration Fields were calculated. To derive these, Residence Times from backward trajectories are summed after scaling by the surface concentration at the release site for the corresponding hour, following [Seibert et al. \(1994\)](#). All the grids of particle paths passing over source regions will therefore be scaled up while clean air trajectories will be scaled to zero so that the final sum will reveal potential source regions. It should be noted however that this method is not able to distinguish between different points along the release path. As a result, the sensitivity of the method is much greater in terms of direction than in terms of distance from the source. Redistribution of Concentration Fields ([Stohl, 1996](#)) was tested for this test case but was not able to converge on a solution and was therefore not used. This was probably because the sources are too spread out and the receptor sites too close to the urban area.

Eulerian pollutant transport was calculated using the Comprehensive Air-quality Model with eXtensions (CAMx, [ENVIRON \(2005\)](#)), version 4.20. This was run on the finest MM5 domain at 3 km resolution with the first 15 of the 23 vertical levels used in MM5. This corresponds to approximately 5200 m above ground and 440 hPa over Mexico City. Chemistry was turned off and the simulation was carried out for just CO and SO₂ acting as passive tracers.

Vertical diffusion is treated with parameterisations based on surface and boundary layer parameters. These were obtained from MM5 which was run with the MRF boundary layer scheme ([Hong and Pan, 1996](#)). The coefficients of [O'Brien \(1970\)](#) (OB70) and of the CMAQ model ([Byun, 1999](#)) were tested in CAMx, but not those based on turbulent kinetic energy as this is not calculated by the MRF scheme.

CAMx version 4.20 had a number of improvements. Of particular relevance was the reduction in the horizontal diffusion and the time interpolation of the vertical diffusion coefficient. The first change led to reduced mixing, but the second led to increased

Sources and transport of CO and SO₂ in the MCMA

B. de Foy et al.

[Title Page](#)[Abstract](#)[Introduction](#)[Conclusions](#)[References](#)[Tables](#)[Figures](#)[⏪](#)[⏩](#)[◀](#)[▶](#)[Back](#)[Close](#)[Full Screen / Esc](#)[Printer-friendly Version](#)[Interactive Discussion](#)

mixing in the morning hours. While these compensated each other to some degree, the earlier mixing improved the concentration profiles during rush-hour.

3 Measurements

3.1 FTIR

5 Mobile column measurements of CO were made using Fourier Transform Infrared Spectroscopy (FTIR). A medium resolution spectrometer (0.5 cm^{-1}) was used with a new 360-degree solar tracker. This system was used to evaluate a number of species both in fixed site mode and in mobile mode to evaluate point source emissions with the Solar Occultation Flux method (SOF). This study makes use of the 126 total CO
10 columns measured between 11 April and 1 May.

The long-path FTIR (LP-FTIR) system at CENICA consisted of a medium resolution (1 cm^{-1}) spectrometer (Bomem MB104) coupled to a custom fabricated transmitting and receiving telescope. At the other side of the light path, a cubecorner array was mounted at a tower, making up a total folded path of 860 m (parallel to DOAS-1 described below). The system provided data with 5-min integration time continuously
15 from 22:20 on 9 March to 00:00 on 29 April, except for a 12 h gap on 11 April. Spectra were analyzed using the latest HITRAN database cross sections (Rothman et al., 2003) and a nonlinear fitting algorithm.

Separate long-path FTIR measurements were made at La Merced as described in Grutter et al. (2005) and Grutter (2003). A Nicolet interferometer was used with a ZnSe beamsplitter operating at 0.5 cm^{-1} resolution. The liquid-nitrogen-cooled MCT detector had a working range of 600 to 4000 cm^{-1} . The equipment was mounted on top of two 4-storey buildings leading to a single path length of 426 m that was 20 m above ground level. Continuous data was available from 1 April to 4 May inclusive for 75% of the time.
20 As for the CENICA FTIR, the spectra were analyzed with the HITRAN cross sections of Rothman et al. (2003).
25

Sources and transport of CO and SO₂ in the MCMA

B. de Foy et al.

Title Page

Abstract

Introduction

Conclusions

References

Tables

Figures

⏪

⏩

◀

▶

Back

Close

Full Screen / Esc

Printer-friendly Version

Interactive Discussion

3.2 Zenith sky UV/Visible spectroscopy

A Mini-DOAS (Differential Optical Absorption Spectrometer) system was deployed. This uses an Ocean Optics spectrometer with operating range of 280 to 390 nm and 0.6 nm resolution using the DOASIS (Kraus, 2001) and WinDoas (Fayt and van Roozendaal, 2001) retrieval software. In mobile mode, columns of SO₂ are obtained along plume traverses. Multiplying the column integrated over the traverse by the average wind speed yields the emission estimates. Wind speed was measured at the ground as well as by dual beam mini-DOAS, with estimated speeds ranging from 3.4 m/s to 7.7 m/s for different traverses.

Six traverses were carried out for the Tula industrial complex on 1 May. This yielded an average estimated emission rate of 4.6 kg/s of SO₂.

On the afternoons of 27 and 28 April, two traverses of the plume of the Popocatepétl volcano yielded an estimate of 9.5 kg/s. Daily summaries of volcanic activity are available from CENAPRED (<http://www.cenapred.unam.mx/>). These report between 2 and 25 low intensity exhalations of steam and gas everyday of the campaign. There were occurrences of small to moderate explosions on 17 April, on 24 to 25 April and on 27 to 28 April. The last episode involved the ejection of incandescent debris to a distance of about 800 m at night and some moderate amplitude tremors. As described above, the volcano is a passively degassing eruptive volcano with continuous SO₂ emissions in the absence of any visible eruptions.

3.3 DOAS

The DOAS technique has been described in Platt (1994). Two long-path DOAS (LP-DOAS) systems were mounted at CENICA. SO₂ was measured by detection of the unique specific narrow-band (5 nm) absorption structures in the ultraviolet spectral range (near 300 nm). Both LP-DOAS were installed on the rooftop of the CENICA building, from where light of a broadband UV/vis lightsource (Xe-short arc lamp) was projected into different directions into the open atmosphere: DOAS-1 pointed towards

Sources and transport of CO and SO₂ in the MCMA

B. de Foy et al.

Title Page

Abstract

Introduction

Conclusions

References

Tables

Figures

◀

▶

◀

▶

Back

Close

Full Screen / Esc

Printer-friendly Version

Interactive Discussion

an array of retro reflectors located in south-easterly direction (TELCEL tower), DOAS-2 pointed towards an array of retro reflectors located in south-westerly direction on top of the local hill Cerro de la Estrella. The lightbeam was folded back into each instrument and spectra were recorded using a Czerny-Turner type spectrometer coupled to a 1024-element PDA detector. The average height of the light path was 16 m and 70 m above ground, the total path length was 860 m and 4.42 km, the mean SO₂ detection limits were 0.26 ppbv and 0.15 ppbv, respectively. SO₂ reference spectra were recorded by introducing a quartz cell filled with SO₂ into a DOAS lightbeam. Spectra were analysed using nonlinear least squares fitting routines by [Fayt and van Roozendaal \(2001\)](#) and [Stutz and Platt \(1996\)](#). and reported concentrations are based on the absorption cross section of [Vandaele et al. \(1994\)](#). Data was available for DOAS-1 from 06:00 on 3 April until 11:00 on 2 May and for DOAS-2 from 00:00 on 3 April to 17:45 on 11 April and from 08:40 on 18 April to 13:30 on 3 May. Other data from DOAS-1 and DOAS-2 is described in [Volkamer et al. \(2005b\)](#) and [Volkamer et al. \(2005a\)](#). At MER, a commercial DOAS system (Opsis) was installed with the same open-path as the FTIR ([Grutter et al., 2005](#)) providing data at 5-min resolution from 1 April to 4 May.

3.4 Monitoring stations

The MCMA-2003 field campaign was based at the National Center for Environmental Research and Training (Centro Nacional de Investigación y Capacitación Ambiental, CENICA) super-site. Figure 1 shows the location of the measurement sites used in this study. A monitoring site measuring meteorological parameters and criteria pollutants is under continuous operation there. In addition, the CENICA mobile van with similar equipment was deployed within the grounds of a primary school in Santa Ana Tlacotenco (SATL). This is a small village on the south-eastern edge of the basin overlooking the MCMA. Surface criteria pollutant concentrations are measured throughout the city by the Ambient Air Monitoring Network (Red Automática de Monitoreo Atmosférico, RAMA). This data was available both at the raw 1-min resolution and in 1-h averages, detailed information on all the stations is available online

Sources and transport of CO and SO₂ in the MCMA

B. de Foy et al.

Title Page

Abstract

Introduction

Conclusions

References

Tables

Figures

◀

▶

◀

▶

Back

Close

Full Screen / Esc

Printer-friendly Version

Interactive Discussion

(<http://www.sma.df.gob.mx/simat/>, see “Mapoteca”).

CO measurements were made using the Teledyne API model 300 CO analyser which uses the gas filter correlation method. Infrared radiation at 4.7 μm passes through a rotating gas filter wheel at 30 Hz. This cycles between the measurement cell containing nitrogen which does not affect the beam before passing through the detection cell, and the reference cell containing a mixture of nitrogen and CO which saturates the beam.

SO₂ measurements were made using pulsed UV fluorescence (Teledyne API models 100 and 100A). UV radiation of 214 nm is passed through the detection cell and the photomultiplier tube is fitted with a filter in the range of 220 to 240 nm.

The timezone in the MCMA was Central Standard Time (CST=UTC−6) before 6 April and daylight saving time (CDT=UTC−5) thereafter. The field campaign policy specified the use of local time for data storage and analysis, a convention that will be followed here with times in CDT unless marked otherwise.

4 Carbon monoxide

Carbon monoxide is emitted mainly by mobile sources and acts as a passive tracer on the time scales of the MCMA. It is therefore a useful quantity to verify the simulated transport by both Lagrangian and Eulerian models. For Lagrangian simulations, Concentration Field analysis can be used to identify possible source regions which can then be compared with known inventories. For Eulerian models, comparisons with surface measurements are used to verify model performance. Column measurements are used to verify the total emissions and to identify potential adjustment factors.

4.1 Concentration field analysis

Concentration field analysis was applied to CO concentrations at three locations: CENICA near the centre of the city, VIF to the north of the MCMA and SATL to the south. In order to increase the sensitivity of the method in the radial distance from the

Sources and transport of CO and SO₂ in the MCMA

B. de Foy et al.

Title Page

Abstract

Introduction

Conclusions

References

Tables

Figures

◀

▶

◀

▶

Back

Close

Full Screen / Esc

Printer-friendly Version

Interactive Discussion

source, it can be applied to multiple stations at once. In order to evaluate the limitations of the method, it is first applied to simulated concentrations obtained from forward runs of the model. Ideally, we would recover the initial emission inventory. Results are shown in Fig. 4. Comparison with the spatial emission map in Fig. 2 shows that the method is able to recover the urban core of the emissions. As expected, there is a high background as the method cannot distinguish distances from the observation sites. Note that this problem is reduced around VIF and SATL, and would be further reduced by adding stations all around the MCMA.

The same map with the actual measured concentrations is also shown in Fig. 4. The method is still able to identify the urban emission in the centre, but the picture is much less focused. There are small but noticeable impacts from wind flows from the Mexican Plateau, from the pass to Toluca and from the Chalco passage. At this point, it is not possible to say if this is due to limitations in the wind simulations, or if it is evidence of impacts from neighbouring airsheds.

Individual Concentration Fields are shown for VIF and SATL in Fig. 5. These stations are removed from local emission sources and are located on the periphery of the MCMA. Results from both stations point to the MCMA urban area as the main emission source, showing that they are able to identify the direction of possible sources. Emission source areas are however much more spread out for the measured concentrations than for the simulated test case, showing the limitations of the method when applied to large diffuse sources that are located close to the measurement sites.

The same analysis was applied to the other RAMA stations with CO monitors. For some stations, e.g. EAC and ATI, the Concentration Fields are similar to those from VIF and SATL, pointing to the urban area. There were two different pitfalls awaiting other stations. At PED, the highest concentrations are due to local emissions during times of low vertical mixing. These occurred at rush hour in the morning hours when the winds are always down hill, coming from areas with no emissions. Limiting the analysis to daylight hours when stronger winds and stronger mixing leads to more transport gave much better results. This problem can be diagnosed by first performing

Sources and transport of CO and SO₂ in the MCMA

B. de Foy et al.

[Title Page](#)[Abstract](#)[Introduction](#)[Conclusions](#)[References](#)[Tables](#)[Figures](#)[◀](#)[▶](#)[◀](#)[▶](#)[Back](#)[Close](#)[Full Screen / Esc](#)[Printer-friendly Version](#)[Interactive Discussion](#)

the analysis with model concentrations, as shown in Fig. 4, which reveals the method's blind spots. The second pitfall is due to the presence of large local sources. These can dominate the signal at all times of the day and reduce any information content of the Concentration Fields.

5 4.2 Eulerian modelling

CAMx simulations from three test cases will be presented. Case 1 was with the OB70 vertical diffusion coefficient and case 2 with the CMAQ coefficients. Case 3 was similar to case 2 with emissions of CO scaled by a factor of 2. The minimum vertical diffusion coefficient was set to $1 \text{ m}^2/\text{s}$ for CMAQ. For OB70, the domain wide minimum was set to $0.1 \text{ m}^2/\text{s}$ and the kvpatch processor was used to reset the minimum in the bottom 500 m layer to $1 \text{ m}^2/\text{s}$ over urban areas and $0.5 \text{ m}^2/\text{s}$ over forests. Simulations were initialised on 31 March 2003 and run for 35 days. Emissions were scaled depending on the type of day. Saturday and Sundays had emissions that were 15% and 30% lower than weekdays. In addition, school vacation days (13 to 25 April 2003 inclusive) were reduced by 10%, Good Friday (18 April) was reduced by 50% and Maundy Thursday (17 April) was reduced by 30%. Initial fields of CO were set to 0.25 ppm at the surface decreasing to 0.125 ppm at the domain top. All boundary and initial conditions for SO₂ were set to 4 ppb. These values were obtained from inspection of boundary site data as well as simulation results from the GEOS-CHEM model (Bey et al., 2001). For CO, they were verified by comparing the model predicted columns with measurements to the north of the MCMA near Teotihuacan and Pachuca and outside the basin on the slopes of the Popocatepetl. The agreement was very good, with values ranging from 2.0×10^{18} to 2.5×10^{18} molecules/cm².

Profiles of vertical diffusion coefficients are shown in Fig. 6 for both the OB70 and CMAQ algorithms. At night, the values correspond to the specified minimum value except for a shallow layer below 500 m with some mixing. The surface CMAQ coefficients are larger, but the surface layer is shallower than for OB70 and the values rapidly drop to the specified minimum value. During the day, the mixed layer develops rapidly with

Sources and transport of CO and SO₂ in the MCMA

B. de Foy et al.

Title Page

Abstract

Introduction

Conclusions

References

Tables

Figures

◀

▶

◀

▶

Back

Close

Full Screen / Esc

Printer-friendly Version

Interactive Discussion

maximum mixing reached between 16:00 and 19:00. The CMAQ coefficients are substantially higher and, more importantly, extend farther upwards than OB70. By 22:00, mixing has returned to the night-time norm although CMAQ has residual mixing in a layer aloft.

5 The statistical performance of the three cases is shown in Fig. 7a using the statistical diagram introduced in [de Foy et al. \(2006b\)](#). The bias is plotted versus the centred root mean square error (RMSE_c, also called Standard Deviation of Errors) for each RAMA CO monitor for the 34 day period from 1 April to 4 May 2003. Also plotted is the standard variation of the model versus that of the measurements, so as to evaluate the variability of the model concentrations and also to provide a comparison point for the RMSE_c values. These show that the OB70 case has the best fit. The CMAQ case has concentrations that are too low. Increasing the emissions removes the bias but leads to higher errors. Figure 7b shows the correlation coefficient and the index of agreement ([Willmott, 1982](#)) split by episode. Model performance varied substantially across the different days of the campaign. The campaign was therefore split into 15 days that performed well (“Good CO”) and 19 days that did less well. “Good CO” days were: 13 to 16 April and 23 April to 4 May excluding 27 April. This includes both O3-South events and the second, and longest, O3-North event. The poorly performing days include the three Cold Surge episodes as well as the first O3-North episode which was the one that followed a period of heavy rains. This suggests that the current model configuration performed better under dry conditions with clear skies and vigorous vertical mixing. Days with cloud and precipitation as well as low Bowen ratios were the poor performers suggesting that further developments will be needed to simulate evapo-transpiration and vertical mixing under more stable conditions. On this graph, the stations are labelled and show a large range of behaviour. MER and IMP are the most accurately represented by a wide margin. These are city centre locations with large emissions surrounding them. Nonetheless, MER is located in a school and IMP in a campus-like environment which shield them from strong sources in the immediate vicinity. Poor performers include stations in the south such as PED and TAX. For PED,

Sources and transport of CO and SO₂ in the MCMA

B. de Foy et al.

[Title Page](#)[Abstract](#)[Introduction](#)[Conclusions](#)[References](#)[Tables](#)[Figures](#)[⏪](#)[⏩](#)[◀](#)[▶](#)[Back](#)[Close](#)[Full Screen / Esc](#)[Printer-friendly Version](#)[Interactive Discussion](#)

the poor performance may be due to shifting emission patterns whereas for TAX it may be due to local sources as this station is located in a major bus transport hub. The statistics diagram can also suggest possible problem areas. Both MIN and SAG are near stations that perform well (MER and XAL, respectively) although their statistics are noticeably worse. This may be due to very local effects that impact one station but not its neighbour – whether due to emissions near-by or to micro-meteorological impacts.

4.2.1 Column measurements

While the statistics suggest that the current emissions with the OB70 scheme perform well, a vertical measurement is necessary to constrain the total emissions. This is provided by the solar FTIR measurements which give a total column count of CO molecules per square centimetre. Figure 8 shows comparisons of measured CO columns with model predicted columns for the three cases. An offset of 0.52×10^{18} molecules/cm² was applied to the model columns to account for the CO above the domain top, based on a free troposphere concentration of 125 ppb.

Agreement between model and observations is particularly good on 15 April. Unlike many urban areas where the columns increase throughout the day, CENICA experiences a steady reduction starting at noon. This is well captured by the model and is due to the increased horizontal wind speed diluting the urban airmass. The cases with the standard emissions both have a good fit with the column observations even though their surface concentration predictions are quite different. The case with increased emissions clearly leads to too much CO in the atmosphere. There was a sharp drop in emissions on 18 April which was Good Friday, a day when all schools and businesses are closed. This can be seen in the measurements and is correctly captured by a 50% scaling factor in the model. The model does not get the slow but steady increase during the day. This is probably because the temporal distribution used was not modified and the emissions followed the usual rush hour pattern. Subjective experience on the day suggests that the city was very quiet in the morning but activity increased steadily

Sources and transport of CO and SO₂ in the MCMA

B. de Foy et al.

Title Page

Abstract

Introduction

Conclusions

References

Tables

Figures

◀

▶

◀

▶

Back

Close

Full Screen / Esc

Printer-friendly Version

Interactive Discussion

during the day. Agreement on 21 April is not nearly as good. This is attributable to the fact that this is a Cold Surge day, with heavy clouds and some rainfall. Performance of the meteorological model was noticeably reduced during such events.

At Santa Ana, the observations show a sharp increase after noon when the urban plume reaches the southern basin rim. In contrast, the model felt the plume several hours earlier and then returned to background levels with the development of the wind jet through the Chalco passage. Columns 20 km to the west at TPN show a later peak and higher values in the afternoon. Likewise, SATL columns the day before (16 April) also show a later peak. This suggests that the discrepancy is caused by too strong southward transport in the morning and too strong a jet from the Chalco passage in the model, but that nonetheless the flow features can be represented by the model.

Finally, columns at La Merced show that the simulated columns of CO are indeed at the right level without any adjustments in emissions. The columns rise and fall under the competing impact of traffic and wind transport. The greater variability of the measurements is probably due to sub-grid scale effects from a combination of local CO sources and small-scale wind fluctuations.

4.2.2 Spatial analysis

Based on the analysis above, the case with unchanged emissions and OB70 vertical diffusion will be retained as the base case for further analysis. Figure 9 shows the bias and error for each station for the 15 days of the “Good CO” episodes. A clear pattern emerges, with positive bias (simulations higher than measurements) for central and south-western stations and negative bias for northern and eastern stations. This can be explained in terms of the growth of the city. The city is constrained on the southern and western edge by the slopes of the basin rim. This leaves growth on the basin floor to the east and especially to the north. The correlation coefficient is highest (smaller bars) in the city centre and decreases on the periphery. While this could be due in part to the stronger signal in the city centre, it may also be indicative of changing spatial emission patterns. In this case, the temporal distribution pattern is also important.

Sources and transport of CO and SO₂ in the MCMA

B. de Foy et al.

Title Page

Abstract

Introduction

Conclusions

References

Tables

Figures

◀

▶

◀

▶

Back

Close

Full Screen / Esc

Printer-friendly Version

Interactive Discussion

Regions far from the urban centre have different driving profiles from the centre but also from each other due to socio-economic variations.

Boxplots of simulated and measured CO concentrations for CENICA and MER are shown in Fig. 10. At MER there is good agreement between the RAMA measurements, the FTIR and the model simulations. CO levels measured by FTIR in the afternoon are lower than the surface RAMA measurements which may be due to the long path of the FTIR. The model simulations lie in between although they should be closer to the long path measurements as they represent a 3 km wide grid cell. At CENICA, the early morning peak is clearly captured by all the measurements. As expected, the open path measurements are lower than the RAMA point measurements. During the rest of the day, the FTIR measurements are higher than the CENICA data but comparable to the RAMA data. This discrepancy should be investigated, especially if the measurements are used for validating the emissions inventory. The CAMx simulation underpredicts the concentrations especially in the morning. This is due to the fact that CENICA is on the edge of the area of high mobile emissions in the current emission inventory. A revised spatial distribution is needed to improve the agreement.

Further diurnal profiles for XAL, AZC, PED and VIF are shown in Fig. 11. At XAL, the pattern is well-captured but the predictions are too low. This is particularly acute in the morning with a delay in the rise of predicted concentrations. At PED, the opposite is true, with too high emissions in the early morning. VIF, to the north of the city, has much lower concentrations. Nonetheless, they are under-predicted by the model suggesting that the emission inventory needs to be expanded to the north.

At AZC, the morning peak starts too soon and rises too high. This illustrates the pitfalls of comparing gridded model results with point measurements. At VAL (not shown), the timing is correct but it drops off much faster than the measurements. As it stands, the model simulation at AZC is in better agreement with the measurements at VAL and the simulation at VAL with the measurements at AZC. Improved metrics could be obtained either by doing a cross-comparison or by comparing the average of the model with the average of the measurements.

Sources and transport of CO and SO₂ in the MCMA

B. de Foy et al.

Title Page

Abstract

Introduction

Conclusions

References

Tables

Figures

◀

▶

◀

▶

Back

Close

Full Screen / Esc

Printer-friendly Version

Interactive Discussion

4.3 Discussion

Because of differences in vertical pollutant concentrations, surface measurements alone are an insufficient means of verifying emission levels of CO. Column measurements provide a necessary constraint on the vertical distribution of pollutants which can be used together with the surface measurements to select appropriate vertical diffusion scheme and hence verify the emission inventory. Because CO can be treated as an inert tracer, it is possible to validate the wind transport from numerical simulations. This can then be applied to all the species in the model.

By using both forward Eulerian modelling and backward Lagrangian trajectories and combining these with surface observations it is possible to evaluate the spatial distribution of the inventory. This method can suggest possible improvements on the scale of sectors of the city comprising dozens of grid cells. It is still relatively crude however and will not be able to resolve features on the scale of individual grid cells. Comparisons of diurnal boxplots at individual stations can be used to evaluate the temporal distribution of the emissions and to suggest modifications by time of day. These temporal profiles vary spatially and can be observed at different stations throughout the city.

Varying emissions during vacations and holidays are an additional source of uncertainty and model under-performance that has not been quantified in the present study. Scaling factors for high and low emission days can be deduced from CO observations. Caution must be exercised as peak CO is representative of emissions preceding the growth of the mixing layer and does not distinguish between emission levels later in the day. The biggest change by day of week and type of day may be the temporal distribution rather than the overall emission level. Further work will need to refine this with traffic count data that can resolve the spatial differences within the MCMA.

Sources and transport of CO and SO₂ in the MCMA

B. de Foy et al.

Title Page

Abstract

Introduction

Conclusions

References

Tables

Figures

◀

▶

◀

▶

Back

Close

Full Screen / Esc

Printer-friendly Version

Interactive Discussion

5 Sulfur dioxide

5.1 Concentration field analysis

Concentration field analysis was performed for SO₂ in the same way as for CO, see Sect. 4. Results for VIF and SATL, the stations most to the north and south respectively, are shown in Fig. 12. Both of these point to a focused source to the northwest of the city. The signal at VIF is particularly clear, with only a small contributions from areas southwest of the station. Because SATL is further away and on the southern edge of the basin rim, the picture is more diffuse. The trace from the northwest is still clearly visible however, with suggested transport southwards along the western edge of the basin.

5.2 Eulerian modelling

CAMx simulations of SO₂ were carried out with the OB70 vertical diffusion scheme. In addition to the point and area sources from the emissions inventory, point sources for the Tula industrial complex and for the Popocatépetl volcano were added as described in Sect. 3. Generic stack parameters were used which do not affect the long range transport of the plume. Emissions were set to 5 kg/s for Tula and 10 kg/s for Popocatépetl and were constant in time.

Figure 13 shows time series at VIF to the north of the city and CENICA to the south-east. In addition to the total measured and simulated SO₂, the simulated contribution of the Tula industrial complex and the volcano are shown. These were calculated separately by simulating individual tracers for each source. Sharp peaks caused by plumes from the large point sources can be clearly seen. At VIF, there are 7 of these above 50 ppb during the campaign. By the time they reach CENICA, their impact is reduced except for events occurring during Cold Surge episodes when vertical mixing is low and transport is directly from the north. The volcano has the potential to impact the city even during the dry season when winds aloft are predominantly westerly. The signal is

Sources and transport of CO and SO₂ in the MCMA

B. de Foy et al.

Title Page

Abstract

Introduction

Conclusions

References

Tables

Figures

⏪

⏩

◀

▶

Back

Close

Full Screen / Esc

Printer-friendly Version

Interactive Discussion

small however and difficult to differentiate from the urban emissions.

The statistics diagram in Fig. 14 show a strong improvement in the simulations when the power plant and the volcano are added to the emission inventory. The variability of the simulated concentrations without Tula and the Popocatépetl is much lower than the measurements, and closer to the one to one line with the point sources. The negative bias is also reduced and errors are a little lower.

Figure 15 shows the comparison in measured and simulated diurnal SO₂ concentrations at CENICA and MER. At CENICA, the monitoring station data is 4 ppb higher than the DOAS measurements. This is believed to be a problem with the monitoring equipment leading to a value of the background that is too high. The DOAS measurements have low levels throughout the day with a morning increase lasting until noon. The RAMA measurements have a stronger diurnal variation with lower levels at night and higher ones during the day. Model simulations have a substantially higher baseline due to the boundary and initial conditions of 4 ppb. The higher-accuracy DOAS measurements suggest that these values be revised downwards. In addition, the reduced diurnal variation of the simulations suggests that local sources are under-represented.

At MER, levels of SO₂ measured by DOAS are similar to those at CENICA. The RAMA measurements however have both a higher base line and a substantially larger morning peak extending into the afternoon. The time-series over the whole month (not shown) gives the impression of a steady day-to-day accumulation in SO₂ levels starting on 22 April. This is not corroborated by neighbouring surface sites or by the DOAS suggesting that it may be an artefact, possibly linked to very local sources. The site is located in a school and the increase corresponds to the end of school vacation. The CAMx simulation has a diurnal peak that is earlier and sharper than the measurements. This is in sharp contrast with CENICA where the diurnal variation of SO₂ was well characterised. This may be due to an over-representation of mobile emissions of SO₂ at MER. It should be noted however that this is in further contrast with the diurnal profiles of CO where CAMx accurately represented the morning peak at MER but had insufficient mobile emissions at CENICA.

Sources and transport of CO and SO₂ in the MCMA

B. de Foy et al.

Title Page

Abstract

Introduction

Conclusions

References

Tables

Figures

◀

▶

◀

▶

Back

Close

Full Screen / Esc

Printer-friendly Version

Interactive Discussion

**Sources and
transport of CO and
SO₂ in the MCMA**B. de Foy et al.

[Title Page](#)[Abstract](#)[Introduction](#)[Conclusions](#)[References](#)[Tables](#)[Figures](#)[⏪](#)[⏩](#)[◀](#)[▶](#)[Back](#)[Close](#)[Full Screen / Esc](#)[Printer-friendly Version](#)[Interactive Discussion](#)

Figure 16 shows diurnal profiles at XAL, AZC, PED and VIF. At XAL, the SO₂ levels are substantially higher than the other stations, which is not captured in the simulations. At PED the observed levels are lower than the simulations. The diurnal profile is different from the CO profile. The increase is more gradual starting at midnight until 09:00 or 10:00, followed by a levelling off or slow decrease until 18:00. Comparing XAL, MER and PED shows the timing of the peak to be later for the southern stations.

The diurnal profile at VIF suggests a similar story to the CO profile, with model emissions underestimated in the new parts of the city. AZC has a peak sharper and earlier than the measurements. As for CO, both the simulations and the measurements are noticeably different at VAL suggesting that local effects play an important role. As for the other stations, the model has a spurious morning peak due to an incorrect temporal emissions profile. In contrast to the DOAS measurements however, the baseline at all the stations is in agreement with the RAMA data. This suggests that the monitoring equipment may over-represent background levels and that caution should be exercised when drawing conclusions about the level of SO₂ emissions in the inventory.

5.3 SO₂ plume event

10 April experienced a large SO₂ plume that swept past the whole city with peak concentrations above 200 ppb in the northern part of the MCMA. Contour plots for 04:00, 07:00 and 10:00 are shown in Fig. 17 for RAMA measurements and model simulations. Figure 18 shows the time series of SO₂ concentrations at points on the northern boundary of the MCMA as well as at different stations along a north–south transect. The initial rise is at TLI, to the west of the Sierra de Guadalupe at around 22:00 of the previous day. Two hours after this there is a substantially larger rise that now extends to VIF to the north, which experiences the bulk of the plume after 03:00. The plume then shifts further east to XAL before returning west to VIF at around sunrise followed by dispersion due to vertical mixing. The impact can be seen at MER building up through the night along with fluctuations due to the plume meandering. At CENICA the levels are lower and smoother due to the longer transport distance. This is accentuated at PED

which starts to see the plume around 03:00 and reaches a maximum between 09:00 and 12:00. Long-path DOAS measurements at CENICA are in remarkable agreement with the point measurement. In addition to adding confidence to the accuracy of the measurements, this highlights the fact that the plume is a large scale phenomenon.

5 Both the measurements and the simulations suggest that the SO₂ plume originated to the north of the MCMA, possibly at the Tula industrial complex.

As can also be seen in the time series in Fig. 13, the timing and extent of the plume is correctly captured although the maximum levels are under-predicted. The measurement contours show the plume going around both sides of the Sierra de Guadalupe and then moving towards the east. In the model, there is some splitting of the plume around the mountains, but the main effect of the Sierra de Guadalupe is to cause strong vertical mixing leading to a much more diffuse plume. This explains the lower levels observed over the city and the reduced extent of an SO₂-rich air mass separated from the plume moving north-eastward at 10:00. This case suggests that the effect of terrain on transport in the stable boundary layer may not be correctly represented numerically.

5.4 Discussion

Both Concentration Field analysis with backward trajectories and forward Eulerian modelling using emission estimates from zenith sky UV spectroscopy suggest that there is a SO₂ plume from the Tula industrial complex that can impact the MCMA. These plumes are typically in the early morning or late evening under stable conditions when wind flows are from the north. While the effect is strongest on the stations in the north of the city, there are occasions where the entire MCMA is affected. In modelling terms, the SO₂ plume presents a valuable case study for the effect of complex terrain on plume transport under stable conditions. Further study into the vertical diffusion as well as the vertical resolution of the dispersion model could be validated from the surface measurements of SO₂.

Possible impacts from volcanic emissions were identified, although the levels are too low to differentiate from ambient measurements. During the dry season, winds aloft are

Sources and transport of CO and SO₂ in the MCMA

B. de Foy et al.

Title Page

Abstract

Introduction

Conclusions

References

Tables

Figures

◀

▶

◀

▶

Back

Close

Full Screen / Esc

Printer-friendly Version

Interactive Discussion

predominantly westerly and transport the emissions away from the city towards Puebla and beyond. During the field campaign the possible effects were found mainly during the Cold Surge episodes which are characterised by southward winds and stable conditions. It should be noted however that volcanic emissions from the Popocatépetl have been reported to be 10 to 100 times larger than the value used in this study, suggesting that much larger impacts are possible during specific episodes.

Annual SO₂ emission estimates for MCMA mobile sources and for the Tula power plant are shown in Table 1. A fleet-average emission factor is derived from long-path DOAS measurements of SO₂ and CO₂ (Volkamer et al., 2005a). Multiplying this by known fuel consumption in the city during April 2003 and scaling to an annual value leads to an emission estimate 20% lower than the official inventory, which is deemed to be within the accuracy of the simulations and the measurements. An estimate of the power plant emissions was obtained by combining the annual fuel consumption and average sulfur content of the fuel. The emissions of the refinery are not included in this estimate. Overall, this is in agreement with the estimate from UV-Spectroscopy plume measurement given the limits of accuracy.

Summing SO₂ impacts at MER and CENICA from model simulations for the Tula and Popocatépetl point sources suggests that 75% of SO₂ concentrations are due to local sources during April 2003, with possibly 20% from the power plant and 5% from the volcano. Furthermore, inspection of the temporal profile suggest that longer range transport from the north of the city does impact the south. It also suggests that the diurnal emissions profile is very different from the CO profile, with continued emissions at night and no early morning peak.

6 Conclusions

Column measurements of CO with solar FTIR were shown to be a necessary supplement to surface measurements when validating pollutant dispersion models and emissions inventories. In the future, it is anticipated that satellite remote sensing will

Sources and transport of CO and SO₂ in the MCMA

B. de Foy et al.

Title Page

Abstract

Introduction

Conclusions

References

Tables

Figures

◀

▶

◀

▶

Back

Close

Full Screen / Esc

Printer-friendly Version

Interactive Discussion

be able to contribute to this function on the urban scale. Mini-DOAS measurements of SO₂ plumes was found to be an effective means of measuring emissions from large point sources. Dispersion modelling using the estimated sources was found to be in agreement with surface measurements of the plume, thereby increasing the confidence in the results.

Air quality models are dependent on the quality of the emission inventory for accurate simulations. In the same manner, feedback from the models can be used in evaluating the emission inventory and suggesting possible improvements. Current simulations of CO are in agreement with the emission estimates of the MCMA subject to the limits of accuracy of both model and measurements. Analysis of the results however suggests that there are spatial distribution issues due to the growth of the city that need to be included. The time series of the simulations also suggest that the temporal profiles of the emissions varies by location within the city as well as with different activity days. SO₂ levels in the city were shown to be influenced by large point sources outside the city.

Large uncertainties exist in the vertical diffusion schemes used by models. Column measurements provide an effective constraint on the emission inventory so that surface concentration measurements can be used in constraining the vertical diffusivity. This reduces the risk of introducing compensating errors, for example increasing the level of emissions to make up for an overly diffusive scheme. Large plumes detected by multiple surface measurement sites provide a useful case study of model dispersion. Flow past a hill during stable conditions suffered from excessive numerical diffusion. This serves as a valuable data set for future model testing. Finally, the combination of backward trajectories and forward Eulerian modelling can be used to test experiment design and observation locations. By simulating the dispersion of the urban plumes, potential observation sites can be tested for their ability to identify both point and area sources.

Carbon monoxide levels are within the health standard at present thanks to reductions in emissions over the last decade, and the current emission inventory was found

Sources and transport of CO and SO₂ in the MCMA

B. de Foy et al.

Title Page

Abstract

Introduction

Conclusions

References

Tables

Figures

⏪

⏩

◀

▶

Back

Close

Full Screen / Esc

Printer-friendly Version

Interactive Discussion

**Sources and
transport of CO and
SO₂ in the MCMA**B. de Foy et al.

[Title Page](#)[Abstract](#)[Introduction](#)[Conclusions](#)[References](#)[Tables](#)[Figures](#)[⏪](#)[⏩](#)[◀](#)[▶](#)[Back](#)[Close](#)[Full Screen / Esc](#)[Printer-friendly Version](#)[Interactive Discussion](#)

to give correct CO levels in the dispersion models. Furthermore, CO can be used as a tracer to validate the pollutant transport in numerical models, giving confidence in the results for applications in photochemical and aerosol modelling. The SO₂ health standard is 30 ppb for the annual average with one 24-h average above 130 ppb per year.

5 Currently, this is met for all the stations, but there is the potential for a 24-h average exceedance due to point sources outside the MCMA. It should also be noted that 1-h averages can reach very high levels which are not yet regulated by a health standard. Finally, SO₂ has an impact on aerosol formation and processing, and correctly simulating SO₂ levels is important for future aerosol simulations and their associated health effects.

10 *Acknowledgements.* The analysis contained in this paper was made possible by the collaborative efforts of many people involved in field measurements, both during the campaign and over longer periods of time. We are indebted to the staff of CENICA who hosted the campaign. We would like to thank S. Blanco, A. Sanchez, O. Fentanes, J. Zaragoza, A. P. Ocampo, C. Cruz, C. Aguirre, R. Romo, A. Pino, R. Castañeda, R. Rodríguez, P. Escamilla. We would also like to thank C. R. Ramos, A. Retama and the operators and analyst personnel of the “Red Automática de Monitoreo Atmosférico del Gobierno del Distrito Federal” for their contribution in administering and gathering the data used in this manuscript.

20 MM5 is made publicly available and supported by the Mesoscale and Microscale Meteorology division at the National Center for Atmospheric Research for which the authors are very grateful. CAMx is made publicly available by ENVIRON, and the authors would like to thank G. Yarwood and C. Emery for their support. The authors thank A. Stohl for making FLEXPART available and G. Wotawa for developing the MM5 version.

25 The financial support of the U.S. National Science Foundation, awards ATM-0511803 and ATM-0528227, is gratefully acknowledged.

References

Ashbaugh, L. L., Malm, W. C., and Sadeh, W. Z.: A residence time probability analysis of sulfur concentrations at grand-canyon-national-park, Atmos. Environ., 19, 1263–1270, 1985.

6131, 6135

Barth, M. C. and Church, A. T.: Regional and global distributions and lifetimes of sulfate aerosols from Mexico city and southeast China, *J. Geophys. Res.-Atmos.*, 104, 30231–30239, 1999. [6130](#)

5 Begum, B. A., Kim, E., Jeong, C. H., Lee, D. W., and Hopke, P. K.: Evaluation of the potential source contribution function using the 2002 Quebec forest fire episode, *Atmos. Environ.*, 39, 3719–3724, 2005. [6132](#)

Berg, L. K. and Zhong, S. Y.: Sensitivity of MM5-simulated boundary layer characteristics to turbulence parameterizations, *J. Appl. Meteorol.*, 44, 1467–1483, 2005. [6133](#)

10 Bey, I., Jacob, D. J., Yantosca, R. M., Logan, J. A., Field, B. D., Fiore, A. M., Li, Q. B., Liu, H. G. Y., Mickley, L. J., and Schultz, M. G.: Global modeling of tropospheric chemistry with assimilated meteorology: Model description and evaluation, *J. Geophys. Res.-Atmos.*, 106, 23073–23095, 2001. [6130](#), [6142](#)

Biswas, J. and Rao, S. T.: Uncertainties in episodic ozone modeling stemming from uncertainties in the meteorological fields, *J. Appl. Meteorol.*, 40, 117–136, 2001. [6134](#)

Blanchard, C. L.: Methods for attributing ambient air pollutants to emission sources, *Ann. Rev. Energy Environ.*, 24, 329–365, 1999. [6131](#)

Brandt, J., Bastrup-Birk, A., Christensen, J. H., Mikkelsen, T., Thykier-Nielsen, S., and Zlatev, Z.: Testing the importance of accurate meteorological input fields and parameterizations in atmospheric transport modelling using DREAM – Validation against ETEX-1, *Atmos. Environ.*, 32, 4167–4186, 1998. [6134](#)

20 Byun, D. W.: Dynamically consistent formulations in meteorological and air quality models for multiscale atmospheric studies. Part I: Governing equations in a generalized coordinate system, *J. Atmos. Sci.*, 56, 3789–3807, 1999. [6136](#)

25 Comisión Ambiental Metropolitana: Inventario de Emisiones de la Zona Metropolitana del Valle de México, Tech. Rep. (Web), Secretaría del Medio Ambiente, Gobierno de México, México, 2004. [6128](#), [6135](#)

de Foy, B., Caetano, E., Magaña, V., Zitácuaro, A., Cárdenas, B., Retama, A., Ramos, R., Molina, L. T., and Molina, M. J.: Mexico City basin wind circulation during the MCMA-2003 field campaign, *Atmos. Chem. Phys.*, 5, 2267–2288, 2005. [6128](#)

30 de Foy, B., Clappier, A., Molina, L. T., and Molina, M. J.: Distinct wind convergence patterns in the Mexico City basin due to the interaction of the gap winds with the synoptic flow, *Atmos. Chem. Phys.*, 6, 1249–1265, 2006a. [6135](#)

ACPD

6, 6125–6181, 2006

Sources and transport of CO and SO₂ in the MCMA

B. de Foy et al.

Title Page

Abstract

Introduction

Conclusions

References

Tables

Figures

◀

▶

◀

▶

Back

Close

Full Screen / Esc

Printer-friendly Version

Interactive Discussion

EGU

- de Foy, B., Molina, L. T., and Molina, M. J.: Satellite-derived land surface parameters for mesoscale modelling of the Mexico City basin, *Atmos. Chem. Phys.*, 6, 1315–1330, 2006b. [6135](#), [6143](#)
- de Foy, B., Varela, J. R., Molina, L. T., and Molina, M. J.: Rapid ventilation of the Mexico City basin and regional fate of the urban plume, *Atmos. Chem. Phys.*, 6, 2321–2335, 2006c. [6128](#), [6135](#)
- Delgado-Granados, H., Gonzalez, L. C., and Sanchez, N. P.: Sulfur dioxide emissions from Popocatepetl volcano (Mexico): case study of a high-emission rate, passively degassing erupting volcano, *J. Volcanol. Geotherm. Res.*, 108, 107–120, 2001. [6129](#)
- Elias, T., Sutton, A. J., Oppenheimer, C., Horton, K. A., Garbeil, H., Tsanev, V., McGonigle, A. J. S., and Williams-Jones, G.: Comparison of COSPEC and two miniature ultraviolet spectrometer systems for SO₂ measurements using scattered sunlight, *Bull. Volcanol.*, 68, 313–322, 2006. [6130](#)
- Elliott, S., Blake, D. R., Rowland, F. S., Lu, R., Brown, M. J., Williams, M. D., Russell, A. G., Bossert, J. E., Streit, G. E., Santoyo, M. R., Guzman, F., Porph, W. M., McNair, L. A., Keyantash, J., Kao, C. Y. J., Turco, R. P., and Eichinger, W. E.: Ventilation of liquefied petroleum gas components from the Valley of Mexico, *J. Geophys. Res.-Atmos.*, 102, 21 197–21 207, 1997. [6127](#)
- ENVIRON: CAMx, comprehensive air quality model with extensions, User's Guide, Tech. Rep. Version 4.20, ENVIRON International Corporation, 2005. [6136](#)
- Fast, J. D. and Zhong, S. Y.: Meteorological factors associated with inhomogeneous ozone concentrations within the Mexico City basin, *J. Geophys. Res.-Atmos.*, 103, 18 927–18 946, 1998. [6127](#)
- Fayt, C. and van Roozendaal, M.: WinDoas 2.1 – Software User Manual, Tech. rep., IASB/BIRA, Belgium, 2001. [6138](#), [6139](#)
- Galindo, I., Ivlev, L. S., Gonzalez, A., and Ayala, R.: Airborne measurements of particle and gas emissions from the December 1994 January 1995 eruption of Popocatepetl Volcano (Mexico), *J. Volcanol. Geotherm. Res.*, 83, 197–217, 1998. [6129](#)
- Galle, B., Oppenheimer, C., Geyer, A., McGonigle, A. J. S., Edmonds, M., and Horrocks, L.: A miniaturised ultraviolet spectrometer for remote sensing of SO₂ fluxes: a new tool for volcano surveillance, *J. Volcanol. Geotherm. Res.*, 119, 241–254, 2003. [6130](#)
- Grell, G. A., Dudhia, J., and Stauffer, D. R.: A Description of the Fifth-Generation Penn State/NCAR Mesoscale Model (MM5), Tech. Rep. NCAR/TN-398+STR, NCAR, 1995. [6135](#)

Sources and transport of CO and SO₂ in the MCMAB. de Foy et al.

Title Page

Abstract

Introduction

Conclusions

References

Tables

Figures

◀

▶

◀

▶

Back

Close

Full Screen / Esc

Printer-friendly Version

Interactive Discussion

- Grutter, M.: Multi-Gas analysis of ambient air using FTIR spectroscopy over Mexico City, *Atmosfera*, 16, 1–13, 2003. [6137](#)
- Grutter, M., Flores, E., Andraca-Ayala, G., and Baez, A.: Formaldehyde levels in downtown Mexico City during 2003, *Atmos. Environ.*, 39, 1027–1034, 2005. [6137](#), [6139](#)
- 5 Hong, S. Y. and Pan, H. L.: Nonlocal boundary layer vertical diffusion in a Medium-Range Forecast Model, *Mon. Wea. Rev.*, 124, 2322–2339, 1996. [6136](#)
- Hopke, P. K.: Recent developments in receptor modeling, *J. Chemom.*, 17, 255–265, 2003. [6131](#)
- 10 Issartel, J. P.: Rebuilding sources of linear tracers after atmospheric concentration measurements, *Atmos. Chem. Phys.*, 3, 2111–2125, 2003. [6132](#)
- Jazcilevich, A. D., García, A. R., and Ruiz-Suarez, L. G.: A study of air flow patterns affecting pollutant concentrations in the Central Region of Mexico, *Atmos. Environ.*, 37, 183–193, 2003. [6127](#)
- Jiang, G. F., Lamb, B., and Westberg, H.: Using back trajectories and process analysis to investigate photochemical ozone production in the Puget Sound region, *Atmos. Environ.*, 37, 1489–1502, 2003. [6133](#)
- 15 Jiang, M., Marr, L. C., Dunlea, E. J., Herndon, S. C., Jayne, J. T., Kolb, C. E., Knighton, W. B., Rogers, T. M., Zavala, M., Molina, L. T., and Molina, M. J.: Vehicle fleet emissions of black carbon, polycyclic aromatic hydrocarbons, and other pollutants measured by a mobile laboratory in Mexico City, *Atmos. Chem. Phys.*, 5, 3377–3387, 2005. [6128](#)
- 20 Jimenez, J. C., Raga, G. B., Baumgardner, D., Castro, T., Rosas, I., Baez, A., and Morton, O.: On the composition of airborne particles influenced by emissions of the volcano Popocatepetl in Mexico, *Nat. Hazards*, 31, 21–37, 2004. [6130](#)
- Kolb, C. E., Herndon, S. C., McManus, B., Shorter, J. H., Zahniser, M. S., Nelson, D. D., Jayne, J. T., Canagaratna, M. R., and Worsnop, D. R.: Mobile laboratory with rapid response instruments for real-time measurements of urban and regional trace gas and particulate distributions and emission source characteristics, *Environ. Sci. Technol.*, 38, 5694–5703, 2004. [6128](#)
- 25 Kraus, S.: The DOASIS Software, in: 1st International DOAS Workshop, Heidelberg, Germany, 2001. [6138](#)
- Kuhns, H., Knipping, E. M., and Vukovich, J. M.: Development of a United States-Mexico emissions inventory for the Big Bend Regional Aerosol and Visibility Observational (BRAVO) Study, *J. Air Waste Manage. Assoc.*, 55, 677–692, 2005. [6129](#)

Sources and transport of CO and SO₂ in the MCMAB. de Foy et al.

[Title Page](#)[Abstract](#)[Introduction](#)[Conclusions](#)[References](#)[Tables](#)[Figures](#)[◀](#)[▶](#)[◀](#)[▶](#)[Back](#)[Close](#)[Full Screen / Esc](#)[Printer-friendly Version](#)[Interactive Discussion](#)

- Lee, H. N. and Larsen, R. J.: Vertical diffusion in the lower atmosphere using aircraft measurements of Rn-222, *J. Appl. Meteorol.*, 36, 1262–1270, 1997. [6133](#)
- Lee, J. H., Hopke, P. K., and Turner, J. R.: Source identification of airborne PM_{2.5} at the St. Louis-Midwest supersite, *J. Geophys. Res.-Atmos.*, 111, DS10S10, doi:10.1029/2002JD006329, 2006. [6133](#)
- Lupu, A. and Maenhaut, W.: Application and comparison of two statistical trajectory techniques for identification of source regions of atmospheric aerosol species, *Atmos. Environ.*, 36, 5607–5618, 2002. [6132](#)
- Marquez, C., Castro, T., Muhlia, A., Moya, M., Martinez-Arroyo, A., and Baez, A.: Measurement of aerosol particles, gases and flux radiation in the Pico de Orizaba National Park, and its relationship to air pollution transport, *Atmos. Environ.*, 39, 3877–3890, 2005. [6130](#)
- McGonigle, A. J. S., Thomson, C. L., Tsanev, V. I., and Oppenheimer, C.: A simple technique for measuring power station SO₂ and NO₂ emissions, *Atmos. Environ.*, 38, 21–25, 2004. [6130](#)
- Molina, L. T. and Molina, M. J. (Eds.): *Air Quality in the Mexico Megacity*, Kluwer Academic Publishers, 2002. [6127](#)
- Molina, L. T., Molina, M. J., Slott, R., Slott, C. E., Gbor, P. K., Meng, F., Singh, R., Galvez, O., Sloan, J. J., Anderson, W., Tang, X. Y., Shao, M., Zhu, T., Zhang, Y. H., Hu, M., Gurjar, B. R., Artaxo, P., Oyola, P., Gramsch, E., Hidalgo, D., and Gertler, A.: 2004 Critical Review Supplement: Air Quality in Selected Megacities, *J. Air Waste Manage. Assoc.*, p. online only, 2004. [6127](#)
- Molina, M. J. and Molina, L. T.: Megacities and atmospheric pollution, *J. Air Waste Manage. Assoc.*, 54, 644–680, 2004. [6127](#)
- Nickerson, E. C., Sosa, G., Hochstein, H., Mccaslin, P., Luke, W., and Schanot, A.: Project Aguila – In situ Measurements of Mexico-City Air-Pollution by a Research Aircraft, *Atmos. Environ. B*, 26, 445–451, 1992. [6127](#)
- Nowacki, P., Samson, P. J., and Sillman, S.: Sensitivity of urban airshed model (UAM-IV) calculated air pollutant concentrations to the vertical diffusion parameterization during convective meteorological situations, *J. Appl. Meteorol.*, 35, 1790–1803, 1996. [6133](#)
- O'Brien, J. J.: A note on the vertical structure of the eddy exchange coefficient in the planetary boundary layer, *J. Atmos. Sci.*, 27, 1214–1215, 1970. [6133](#), [6136](#)
- Olivie, D. J. L., van Velthoven, P. F. J., and Beljaars, A. C. M.: Evaluation of archived and off-line diagnosed vertical diffusion coefficients from ERA-40 with Rn-222 simulations, *Atmos.*

Sources and transport of CO and SO₂ in the MCMAB. de Foy et al.

[Title Page](#)[Abstract](#)[Introduction](#)[Conclusions](#)[References](#)[Tables](#)[Figures](#)[◀](#)[▶](#)[◀](#)[▶](#)[Back](#)[Close](#)[Full Screen / Esc](#)[Printer-friendly Version](#)[Interactive Discussion](#)

- Chem. Phys., 4, 2313–2336, 2004. [6133](#)
- Olivier, J. G. J. and Berdowski, J. J. M.: Global emissions sources and sinks, in: The Climate System, edited by: Berdowski, J., Guicherit, R., and Heij, B. J., pp. 33–78, A. A. Balkema Publishers/Swets and Zeitlinger Publishers, Lisse, The Netherlands, 2001. [6129](#)
- 5 Perez-Roa, R., Castro, J., Jorquera, H., Perez-Correa, J. R., and Vesovic, V.: Air-pollution modelling in an urban area: Correlating turbulent diffusion coefficients by means of an artificial neural network approach, Atmos. Environ., 40, 109–125, 2006. [6134](#)
- Platt, U.: Differential Optical Absorption Spectroscopy, in: Monitoring by Spectroscopic Techniques, edited by: Sigrist, M. W., chap. 2, pp. 27–84, Wiley & Sons, New York, 1994. [6138](#)
- 10 Pyle, D. M. and Mather, T. A.: The regional influence of volcanic emissions from Popocateptl, Mexico: Discussion of “Measurement of aerosol particles, gases and flux radiation in the Pico de Orizaba National Park, and its relationship to air pollution transport”, by Marquez, C., Castro, T., Muhlia, A., et al., 2005, Atmos. Environ., 39, 3877–3890, Atmos. Environ., 39, 6475–6478, 2005. [6130](#)
- 15 Raga, G. B., Kok, G. L., Baumgardner, D., Baez, A., and Rosas, I.: Evidence for volcanic influence on Mexico City aerosols, Geophys. Res. Lett., 26, 1149–1152, 1999. [6130](#)
- Roelofs, G. J., Scheeren, H. A., Heland, J., Ziereis, H., and Lelieveld, J.: A model study of ozone in the eastern Mediterranean free troposphere during MINOS (August 2001), Atmos. Chem. Phys., 3, 1199–1210, 2003. [6134](#)
- 20 Rothman, L. S., Barbe, A., Benner, D. C., Brown, L. R., Camy-Peyret, C., Carleer, M. R., Chance, K., Clerbaux, C., Dana, V., Devi, V. M., Fayt, A., Flaud, J. M., Gamache, R. R., Goldman, A., Jacquemart, D., Jucks, K. W., Lafferty, W. J., Mandin, J. Y., Massie, S. T., Nemtchinov, V., Newnham, D. A., Perrin, A., Rinsland, C. P., Schroeder, J., Smith, K. M., Smith, M. A. H., Tang, K., Toth, R. A., Auwera, J. V., Varanasi, P., and Yoshino, K.: The HITRAN molecular spectroscopic database: edition of 2000 including updates through 2001, J. Quant. Spectr. Radiat. Transfer, 82, 5–44, 2003. [6137](#)
- 25 Sanchez-Ccoyllo, O. R., Dias, P. L. S., Andrade, M. D., and Freitas, S. R.: Determination of O-3-, CO- and PM10-transport in the metropolitan area of Sao Paulo, Brazil through synoptic-scale analysis of back trajectories, Meteorol. Atmos. Phys., 92, 83–93, 2006. [6133](#)
- 30 Schifter, I., Diaz, L., Mugica, V., and Lopez-Salinas, E.: Fuel-based motor vehicle emission inventory for the metropolitan area of Mexico city, Atmos. Environ., 39, 931–940, 2005. [6128](#)
- Seibert, P., Kromp-Kolb, H., Baltensperger, U., Jost, D. T., and Schwikowski, M.: Trajectory analysis of high-alpine air pollution data, in: Air Pollution Modelling and its Application X,

**Sources and
transport of CO and
SO₂ in the MCMA**B. de Foy et al.

Title Page

Abstract

Introduction

Conclusions

References

Tables

Figures

◀

▶

◀

▶

Back

Close

Full Screen / Esc

Printer-friendly Version

Interactive Discussion

edited by: Gryning, S.-E. and Millan, M. M., pp. 595–596, Plenum Press, New York, 1994.

[6132](#), [6136](#)

Sirois, A. and Bottenheim, J. W.: Use of backward trajectories to interpret the 5-year record of pan and o-3 ambient air concentrations at Kejimikujik national park, Nova-Scotia, J. Geophys. Res.-Atmos., 100, 2867–2881, 1995. [6131](#)

Stohl, A.: Trajectory statistics – A new method to establish source-receptor relationships of air pollutants and its application to the transport of particulate sulfate in Europe, Atmos. Environ., 30, 579–587, 1996. [6132](#), [6136](#)

Stohl, A.: Computation, accuracy and applications of trajectories – A review and bibliography, Atmos. Environ., 32, 947–966, 1998. [6132](#)

Stohl, A., Eckhardt, S., Forster, C., James, P., Spichtinger, N., and Seibert, P.: A replacement for simple back trajectory calculations in the interpretation of atmospheric trace substance measurements, Atmos. Environ., 36, 4635–4648, 2002. [6133](#)

Stohl, A., Forster, C., Frank, A., Seibert, P., and Wotawa, G.: Technical note: The Lagrangian particle dispersion model FLEXPART version 6.2, Atmos. Chem. Phys., 5, 2461–2474, 2005. [6135](#)

Stutz, J. and Platt, U.: Numerical analysis and estimation of the statistical error of differential optical absorption spectroscopy measurements with least-squares methods, Appl. Opt., 35, 6041–6053, 1996. [6139](#)

Ulke, A. G. and Andrade, M. F.: Modeling urban air pollution in Sao Paulo, Brazil: sensitivity of model predicted concentrations to different turbulence parameterizations, Atmos. Environ., 35, 1747–1763, 2001. [6134](#)

Vandaele, A. C., Simon, P. C., Guilmot, J. M., Carleer, M., and Colin, R.: SO₂ absorption cross-section measurement in the UV using a fourier-transform spectrometer, J. Geophys. Res.-Atmos., 99, 25 599–25 605, 1994. [6139](#)

Vasconcelos, L. A. D., Kahl, J. D. W., Liu, D. S., Macias, E. S., and White, W. H.: A tracer calibration of back trajectory analysis at the Grand Canyon, J. Geophys. Res.-Atmos., 101, 19 329–19 335, 1996a. [6131](#)

Vasconcelos, L. A. D., Kahl, J. D. W., Liu, D. S., Macias, E. S., and White, W. H.: Spatial resolution of a transport inversion technique, J. Geophys. Res.-Atmos., 101, 19 337–19 342, 1996b. [6132](#)

Volkamer, R., Molina, L. T., Molina, M. J., Flores, E., Grutter, M., Galle, B., Mellqvist, J., Samuelsson, J., Knighton, B., and Jobson, B. T.: Open-path emission factors derived from

ACPD

6, 6125–6181, 2006

Sources and transport of CO and SO₂ in the MCMA

B. de Foy et al.

Title Page

Abstract

Introduction

Conclusions

References

Tables

Figures

◀

▶

◀

▶

Back

Close

Full Screen / Esc

Printer-friendly Version

Interactive Discussion

EGU

- DOAS and FTIR measurements in the Mexico City Metropolitan Area, in: Air Pollution as a Climate Forcing: A Second Workshop, 2005a. [6139](#), [6152](#)
- Volkamer, R., Molina, L. T., Molina, M. J., Shirley, T., and Brune, W. H.: DOAS measurement of glyoxal as an indicator for fast VOC chemistry in urban air, *Geophys. Res. Lett.*, 32, L08806, doi:10.1029/2005GL022616, 2005b. [6139](#)
- West, J. J., Zavala, M. A., Molina, L. T., Molina, M. J., San Martini, F., McRae, G. J., Sosa-Iglesias, G., and Arriaga-Colina, J. L.: Modeling ozone photochemistry and evaluation of hydrocarbon emissions in the Mexico City metropolitan area, *J. Geophys. Res.-Atmos.*, 109, D19312, doi:10.1029/2004JD004614, 2004. [6127](#), [6128](#), [6135](#)
- Williams, M. D., Brown, M. J., Cruz, X., Sosa, G., and Streit, G.: Development and testing of meteorology and air dispersion models for Mexico City, *Atmos. Environ.*, 29, 2929, 1995. [6127](#)
- Willmott, C. J.: Some comments on the evaluation of model performance, *Bull. Amer. Meteorol. Soc.*, 63, 1309–1313, 1982. [6143](#)
- Wotawa, G. and Kroger, H.: Testing the ability of trajectory statistics to reproduce emission inventories of air pollutants in cases of negligible measurement and transport errors, *Atmos. Environ.*, 33, 3037–3043, 1999. [6132](#)
- Wotawa, G. and Trainer, M.: The influence of Canadian forest fires on pollutant concentrations in the United States, *Science*, 288, 324–328, 2000. [6132](#)
- Wright, R., Cruz-Reyna, S. D. L., Harris, A., Flynn, L., and Gomez-Palacios, J. J.: Infrared satellite monitoring at Popocatepetl: Explosions, exhalations, and cycles of dome growth, *J. Geophys. Res.-Solid Earth*, 107(B8), 2153, doi:10.1029/2000JB000125, 2002. [6129](#)
- Yurganov, L. N., Blumenstock, T., Grechko, E. I., Hase, F., Hyer, E. J., Kasischke, E. S., Koike, M., Kondo, Y., Kramer, I., Leung, F. Y., Mahieu, E., Mellqvist, J., Notholt, J., Novelli, P. C., Rinsland, C. P., Scheel, H. E., Schulz, A., Strandberg, A., Sussmann, R., Tanimoto, H., Velazco, V., Zander, R., and Zhao, Y.: A quantitative assessment of the 1998 carbon monoxide emission anomaly in the Northern Hemisphere based on total column and surface concentration measurements, *J. Geophys. Res.-Atmos.*, 109, D15305, doi:10.1029/2004JD004559, 2004. [6130](#)
- Yurganov, L. N., Duchatelet, P., Dzhola, A. V., Edwards, D. P., Hase, F., Kramer, I., Mahieu, E., Mellqvist, J., Notholt, J., Novelli, P. C., Rockmann, A., Scheel, H. E., Schneider, M., Schulz, A., Strandberg, A., Sussmann, R., Tanimoto, H., Velazco, V., Drummond, J. R., and Gille, J. C.: Increased Northern Hemispheric carbon monoxide burden in the troposphere in 2002

Sources and transport of CO and SO₂ in the MCMA

B. de Foy et al.

[Title Page](#)[Abstract](#)[Introduction](#)[Conclusions](#)[References](#)[Tables](#)[Figures](#)[◀](#)[▶](#)[◀](#)[▶](#)[Back](#)[Close](#)[Full Screen / Esc](#)[Printer-friendly Version](#)[Interactive Discussion](#)

and 2003 detected from the ground and from space, *Atmos. Chem. Phys.*, 5, 563–573, 2005. [6130](#)

Zavala, M., Herndon, S. C., Slott, R. S., Dunlea, E. J., Marr, L. C., Shorter, J. H., Zahniser, M., Knighton, W. B., Rogers, T. M., Kolb, C. E., Molina, L. T., and Molina, M. J.: Characterization of on-road vehicle emissions in the Mexico City Metropolitan Area using a mobile laboratory in chase and fleet average measurement modes during the MCMA-2003 field campaign, *Atmos. Chem. Phys. Discuss.*, 6, 4689–4725, 2006. [6128](#)

Zhong, S. Y. and Fast, J.: An evaluation of the MM5, RAMS, and Meso-Eta models at subkilometer resolution using VTMX field campaign data in the Salt Lake Valley, *Mon. Wea. Rev.*, 131, 1301–1322, 2003. [6133](#)

Zhou, L. M., Hopke, P. K., and Liu, W.: Comparison of two trajectory based models for locating particle sources for two rural New York sites, *Atmos. Environ.*, 38, 1955–1963, 2004. [6132](#)

Sources and transport of CO and SO₂ in the MCMA

B. de Foy et al.

Title Page

Abstract

Introduction

Conclusions

References

Tables

Figures

◀

▶

◀

▶

Back

Close

Full Screen / Esc

Printer-friendly Version

Interactive Discussion

Sources and transport of CO and SO₂ in the MCMA

B. de Foy et al.

Table 1. SO₂ annual emissions estimates from fuel consumption in the MCMA and at the Tula power plant compared with the official inventory for the MCMA and the Mini-DOAS estimate for the Tula industrial complex.

	MCMA	Tula Power Plant
Fuel Consumption (metric tons/yr)	5.7×10^6	1.49×10^6
Emission Factor (kg SO ₂ /ton fuel)	0.71	86.26
Annual SO ₂ Emissions (metric tons/yr)	4050	128 000
CAM 2000 Inventory	4929	
Mini-DOAS Estimate		145 000

Title Page

Abstract

Introduction

Conclusions

References

Tables

Figures

◀

▶

◀

▶

Back

Close

Full Screen / Esc

Printer-friendly Version

Interactive Discussion

Sources and transport of CO and SO₂ in the MCMA

B. de Foy et al.

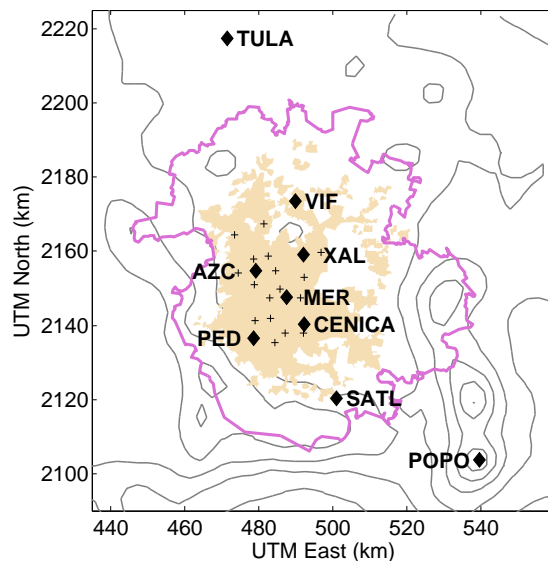


Fig. 1. Map of the MCMA showing the Tula industrial complex, Popocatépetl volcano, CENICA supersite, Santa Ana Tlacotenco (SATL) boundary site and RAMA surface sites (crosses, see Fig. 9 for additional station names). Political border of the MCMA as of 2003 in pink, urban area in beige, terrain contour every 500 m.

[Title Page](#)[Abstract](#)[Introduction](#)[Conclusions](#)[References](#)[Tables](#)[Figures](#)[◀](#)[▶](#)[◀](#)[▶](#)[Back](#)[Close](#)[Full Screen / Esc](#)[Printer-friendly Version](#)[Interactive Discussion](#)

**Sources and
transport of CO and
SO₂ in the MCMA**

B. de Foy et al.

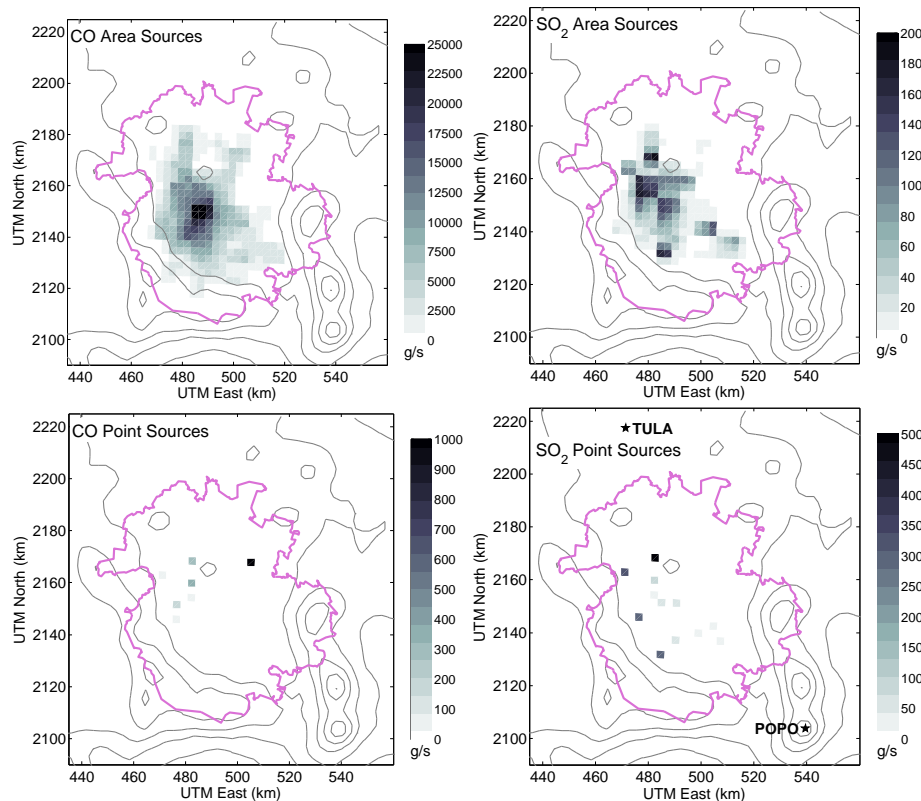


Fig. 2. Daily emission totals for CO (left) and SO₂ (right) from area (top) and point sources (bottom). Point sources are summed to the same grid as the area sources for ease of comparison. Note different scale for each plot. Location of Tula and Popocatépetl shown by the star (not colour coded).

[Title Page](#)[Abstract](#)[Introduction](#)[Conclusions](#)[References](#)[Tables](#)[Figures](#)[◀](#)[▶](#)[◀](#)[▶](#)[Back](#)[Close](#)[Full Screen / Esc](#)[Printer-friendly Version](#)[Interactive Discussion](#)

Sources and transport of CO and SO₂ in the MCMA

B. de Foy et al.

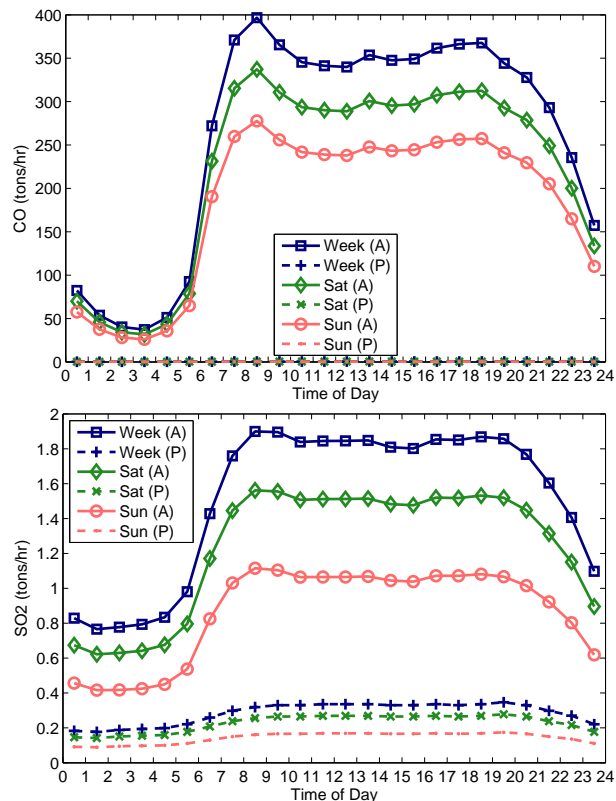


Fig. 3. Diurnal emission profiles for CO and SO₂ from area (A) and point (P) sources summed over the entire simulation domain for weekdays and week-end days. Tula industrial complex and Popocatépetl not included.

[Title Page](#)[Abstract](#)[Introduction](#)[Conclusions](#)[References](#)[Tables](#)[Figures](#)[◀](#)[▶](#)[◀](#)[▶](#)[Back](#)[Close](#)[Full Screen / Esc](#)[Printer-friendly Version](#)[Interactive Discussion](#)

Sources and transport of CO and SO₂ in the MCMA

B. de Foy et al.

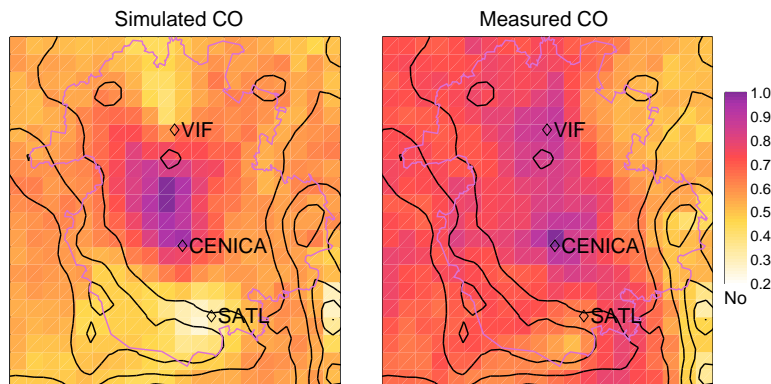


Fig. 4. Concentration Field analysis of CO using simulated (left) and measured (right) time series of concentrations at CENICA, VIF and SATL based on back-trajectories every 2 h at each location. High non-dimensional number (purple) indicates possible source regions, low numbers (white) indicate areas with low emissions.

[Title Page](#)[Abstract](#)[Introduction](#)[Conclusions](#)[References](#)[Tables](#)[Figures](#)[◀](#)[▶](#)[◀](#)[▶](#)[Back](#)[Close](#)[Full Screen / Esc](#)[Printer-friendly Version](#)[Interactive Discussion](#)

Sources and transport of CO and SO₂ in the MCMA

B. de Foy et al.

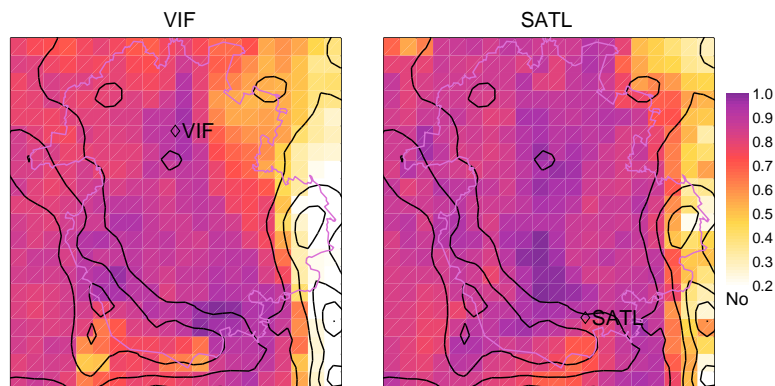


Fig. 5. Concentration Field analysis of CO with measured concentrations at VIF (left) and SATL (right).

Title Page

Abstract

Introduction

Conclusions

References

Tables

Figures

◀

▶

◀

▶

Back

Close

Full Screen / Esc

Printer-friendly Version

Interactive Discussion

Sources and transport of CO and SO₂ in the MCMA

B. de Foy et al.

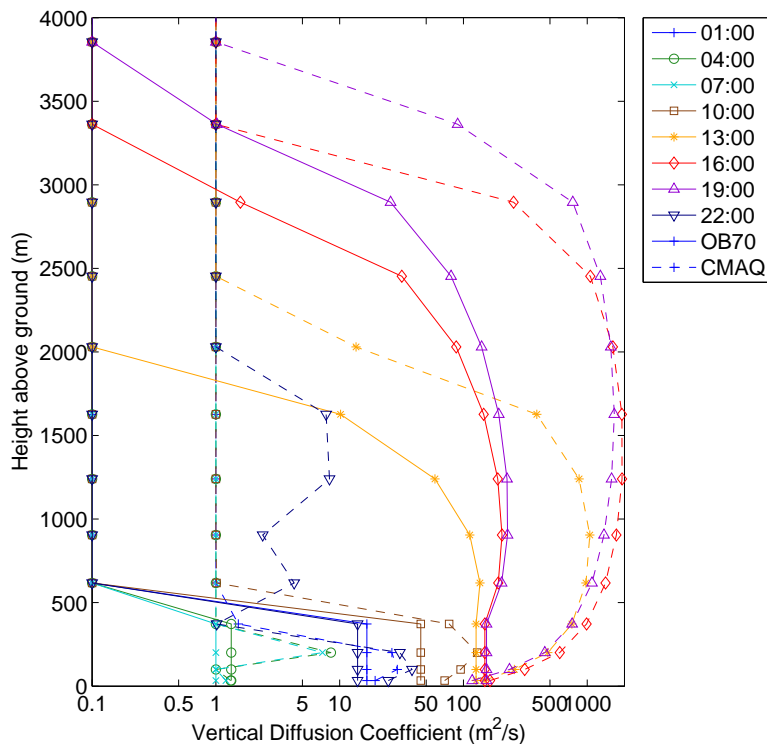


Fig. 6. Comparison of vertical diffusion coefficients at MER from the OB70 (-) and CMAQ (-) algorithms by time of day for 15 April 2003. Values obtained from the CAMx pre-processor for MM5 results using the MRF boundary layer scheme. See text for treatment of minimum value. Note the log scale.

[Title Page](#)[Abstract](#)[Introduction](#)[Conclusions](#)[References](#)[Tables](#)[Figures](#)[◀](#)[▶](#)[◀](#)[▶](#)[Back](#)[Close](#)[Full Screen / Esc](#)[Printer-friendly Version](#)[Interactive Discussion](#)

Sources and transport of CO and SO₂ in the MCMA

B. de Foy et al.

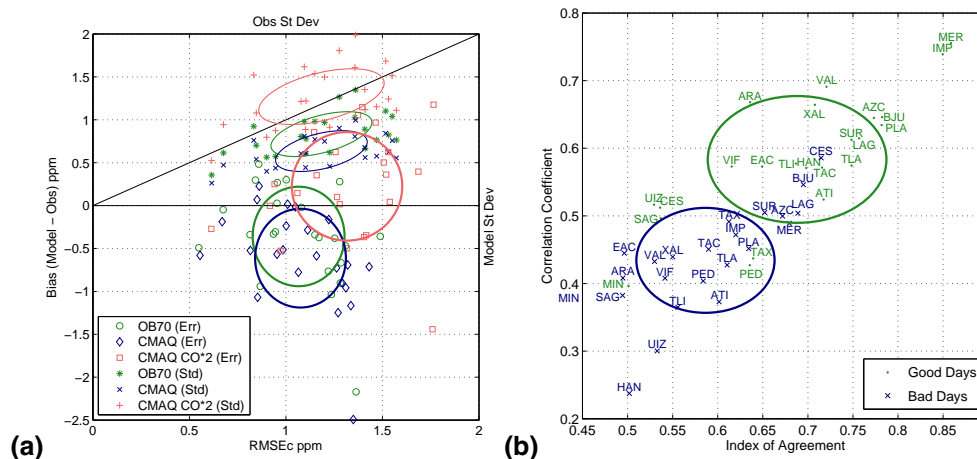


Fig. 7. (a) Statistics diagram for surface CO for 3 cases for all stations with available data for the entire duration of the campaign. Each error point (Err) represents the bias versus the RMSEc (Standard deviation of errors) at a measurement station. Standard deviation points (Std) show the model standard deviation versus that of the measurements, which should be of similar magnitude. (b) Correlation coefficients versus Index of Agreement for the OB70 case separated into “Good CO” days and other days, with stations labelled.

Title Page

Abstract

Introduction

Conclusions

References

Tables

Figures

◀

▶

◀

▶

Back

Close

Full Screen / Esc

Printer-friendly Version

Interactive Discussion

Sources and transport of CO and SO₂ in the MCMA

B. de Foy et al.

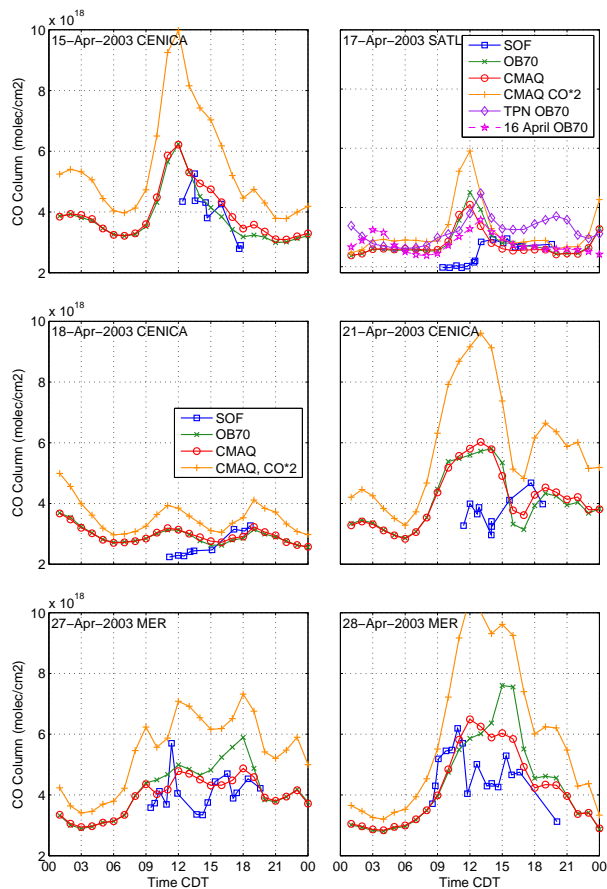


Fig. 8. Total column of CO measured by Solar Occultation Flux (SOF) versus model simulations for different campaign days and sites.

Title Page

Abstract

Introduction

Conclusions

References

Tables

Figures

◀

▶

◀

▶

Back

Close

Full Screen / Esc

Printer-friendly Version

Interactive Discussion

Sources and transport of CO and SO₂ in the MCMA

B. de Foy et al.

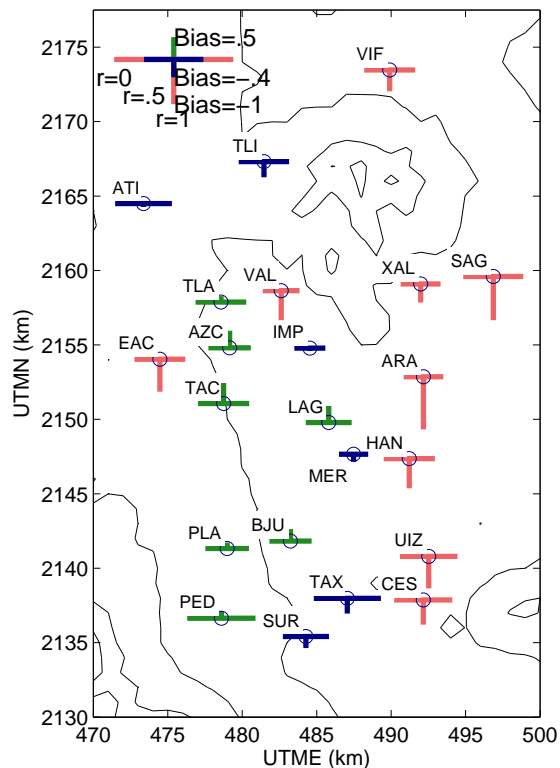


Fig. 9. Bias (vertical lines) and correlation coefficient (horizontal lines) CAMx OB70 vs. RAMA measurements for all stations except MIN, for “Good CO” days. Green for positive bias (model greater than observations), blue for negative bias smaller than 0.4 ppm and red for large negative bias. Correlation coefficient is plotted symmetrically around the origin, short horizontal bars indicate good agreement.

Title Page

Abstract

Introduction

Conclusions

References

Tables

Figures

◀

▶

◀

▶

Back

Close

Full Screen / Esc

Printer-friendly Version

Interactive Discussion

Sources and transport of CO and SO₂ in the MCMA

B. de Foy et al.

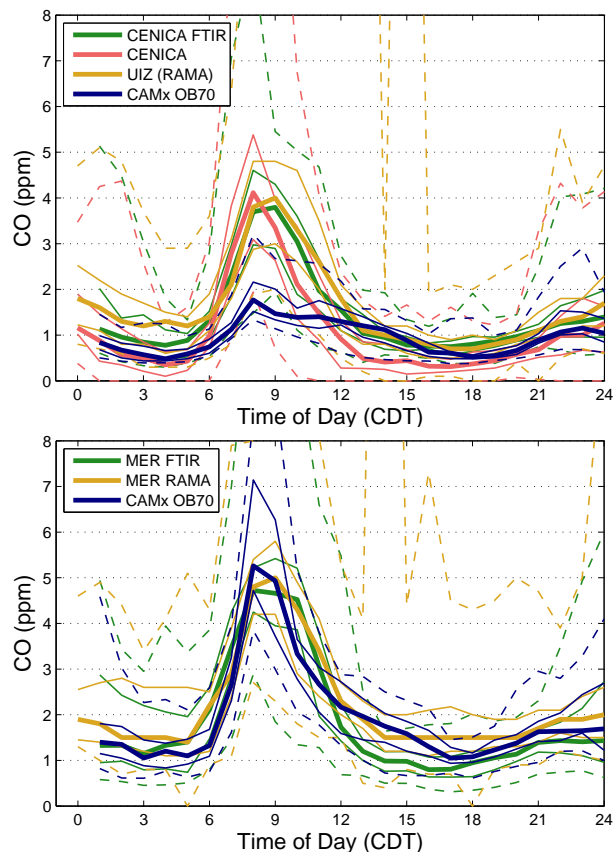


Fig. 10. Diurnal profiles of CO at MER and CENICA comparing monitoring data, FTIR data and CAMx results for “Good CO” days. Bold line is the median, thin line the 25 and 75 percentile and dashed line the range. RAMA measurements in yellow, model simulations in blue.

[Title Page](#)[Abstract](#)[Introduction](#)[Conclusions](#)[References](#)[Tables](#)[Figures](#)[◀](#)[▶](#)[◀](#)[▶](#)[Back](#)[Close](#)[Full Screen / Esc](#)[Printer-friendly Version](#)[Interactive Discussion](#)

Sources and transport of CO and SO₂ in the MCMA

B. de Foy et al.

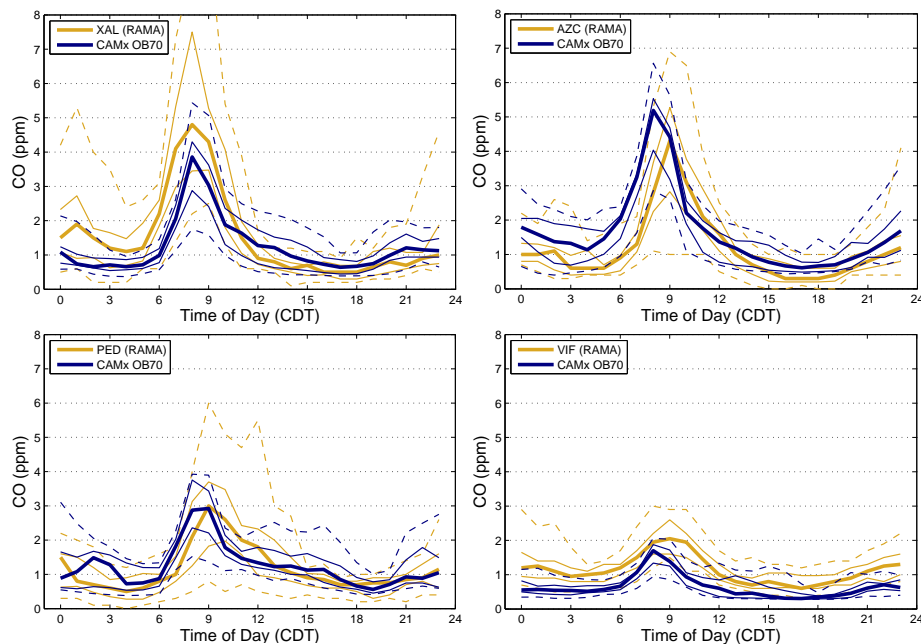


Fig. 11. Diurnal profiles of CO at selected RAMA stations for “Good CO” days. Bold line is the median, thin line the 25 and 75 percentile and dashed line the range. Measurements in yellow, model simulations in blue.

[Title Page](#)[Abstract](#)[Introduction](#)[Conclusions](#)[References](#)[Tables](#)[Figures](#)[◀](#)[▶](#)[◀](#)[▶](#)[Back](#)[Close](#)[Full Screen / Esc](#)[Printer-friendly Version](#)[Interactive Discussion](#)

Sources and transport of CO and SO₂ in the MCMA

B. de Foy et al.

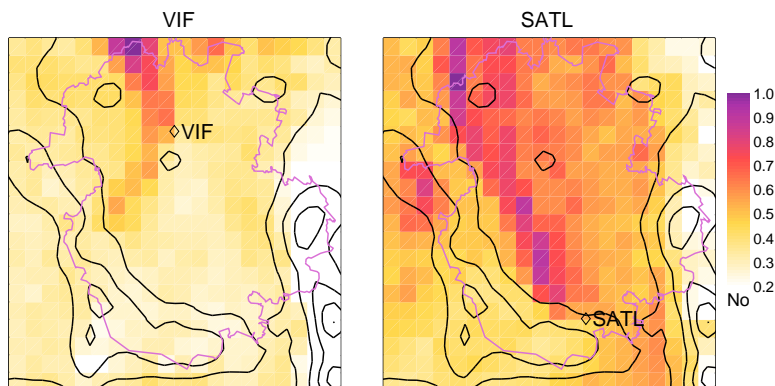


Fig. 12. Concentration Field analysis of SO₂ based on measured concentrations and simulated back-trajectories at VIF (left) and SATL (right) showing possible northwest source region.

[Title Page](#)[Abstract](#)[Introduction](#)[Conclusions](#)[References](#)[Tables](#)[Figures](#)[◀](#)[▶](#)[◀](#)[▶](#)[Back](#)[Close](#)[Full Screen / Esc](#)[Printer-friendly Version](#)[Interactive Discussion](#)

Sources and transport of CO and SO₂ in the MCMA

B. de Foy et al.

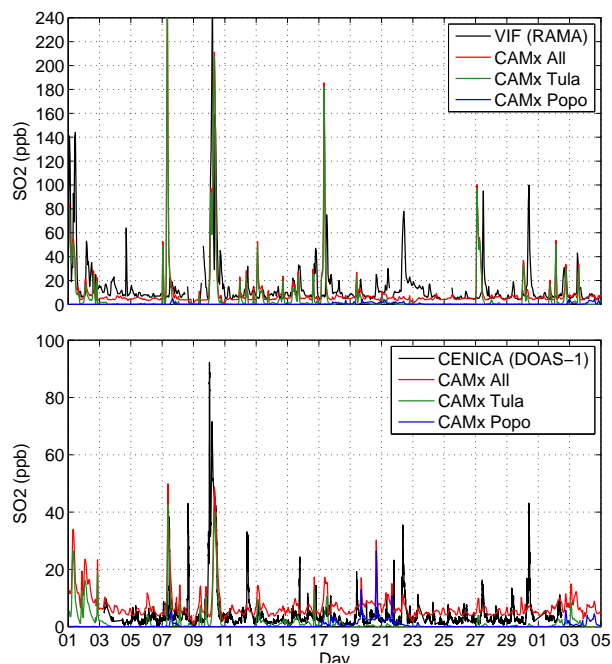


Fig. 13. SO₂ time series at VIF and CENICA showing measured versus modelled concentrations for the entire campaign. Modelled concentrations are further split into impacts from Tula and Popocatépetl.

[Title Page](#)[Abstract](#)[Introduction](#)[Conclusions](#)[References](#)[Tables](#)[Figures](#)[◀](#)[▶](#)[◀](#)[▶](#)[Back](#)[Close](#)[Full Screen / Esc](#)[Printer-friendly Version](#)[Interactive Discussion](#)

Sources and transport of CO and SO₂ in the MCMA

B. de Foy et al.

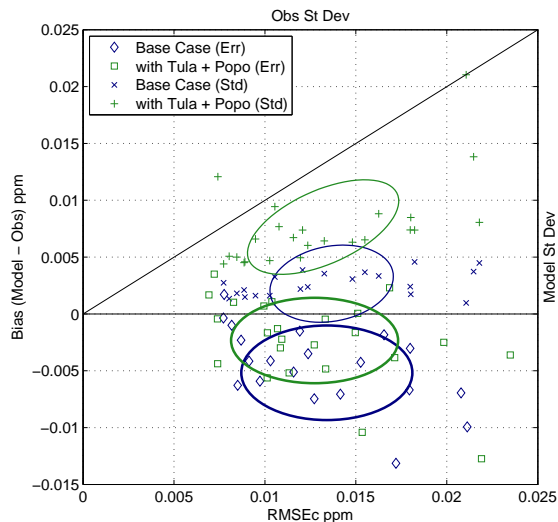


Fig. 14. Statistics diagram for SO₂ comparing simulated concentrations using CAMx and OB70 vertical diffusion with all available RAMA measurements for the entire campaign. The base case uses the official emission inventory, the modified case includes the Tula and the Popocatépetl emissions. Error points show bias versus RMSEc, Std points show model standard deviation versus that of the measurements (see Fig. 7).

[Title Page](#)[Abstract](#)[Introduction](#)[Conclusions](#)[References](#)[Tables](#)[Figures](#)[◀](#)[▶](#)[◀](#)[▶](#)[Back](#)[Close](#)[Full Screen / Esc](#)[Printer-friendly Version](#)[Interactive Discussion](#)

Sources and transport of CO and SO₂ in the MCMA

B. de Foy et al.

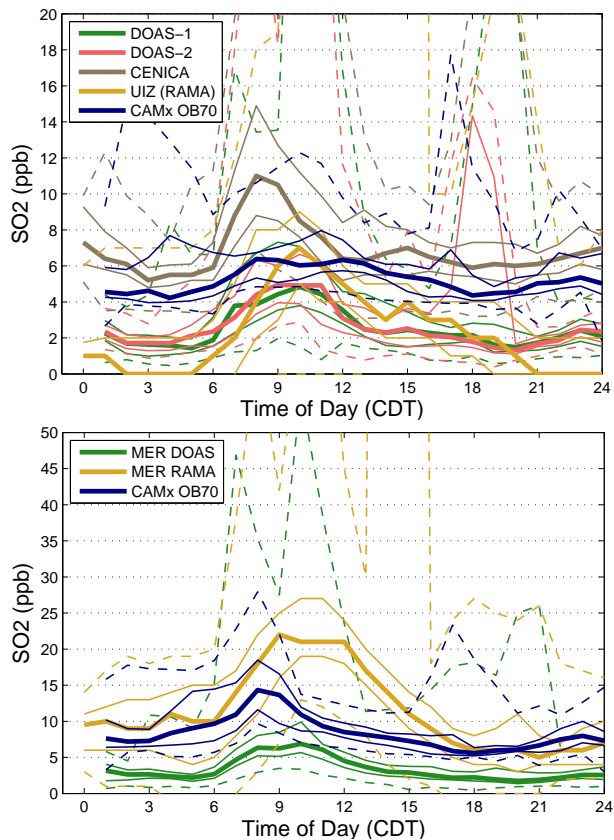


Fig. 15. Diurnal profiles of SO₂ at MER and CENICA comparing monitoring data, DOAS data and model results for “Good CO” days, as for Fig. 10.

[Title Page](#)[Abstract](#)[Introduction](#)[Conclusions](#)[References](#)[Tables](#)[Figures](#)[◀](#)[▶](#)[◀](#)[▶](#)[Back](#)[Close](#)[Full Screen / Esc](#)[Printer-friendly Version](#)[Interactive Discussion](#)

Sources and transport of CO and SO₂ in the MCMA

B. de Foy et al.

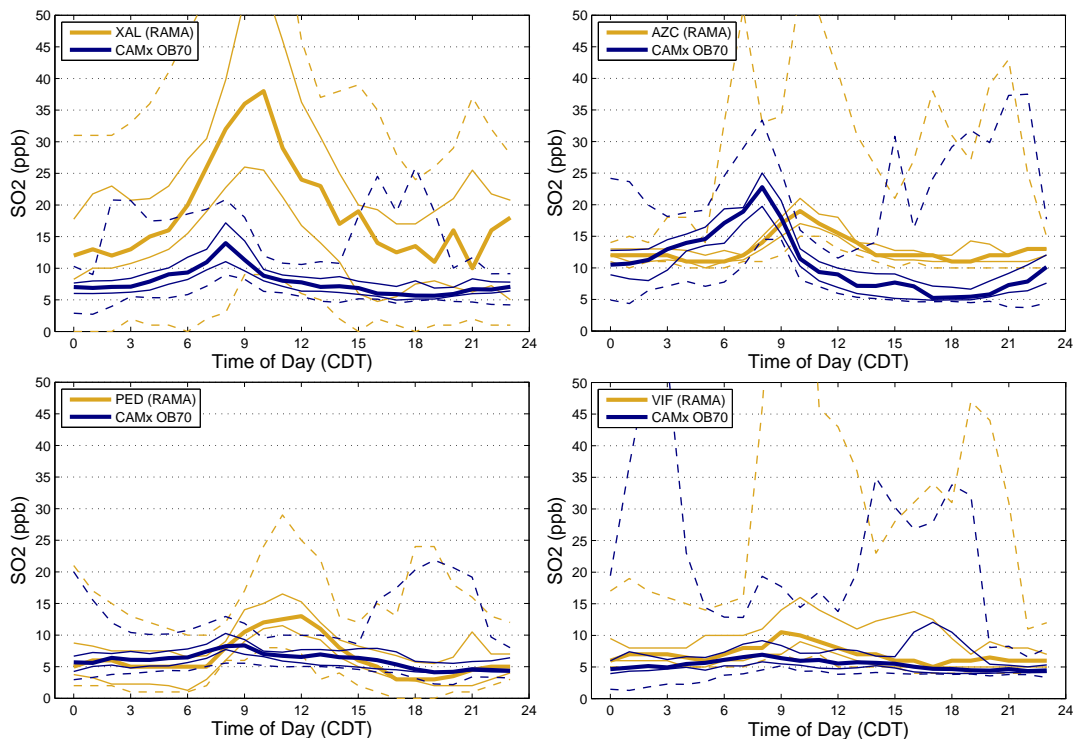


Fig. 16. Diurnal profiles of SO₂ at selected RAMA stations for “Good CO” days, as for Fig. 11.

[Title Page](#)[Abstract](#)[Introduction](#)[Conclusions](#)[References](#)[Tables](#)[Figures](#)[◀](#)[▶](#)[◀](#)[▶](#)[Back](#)[Close](#)[Full Screen / Esc](#)[Printer-friendly Version](#)[Interactive Discussion](#)

Sources and transport of CO and SO₂ in the MCMA

B. de Foy et al.

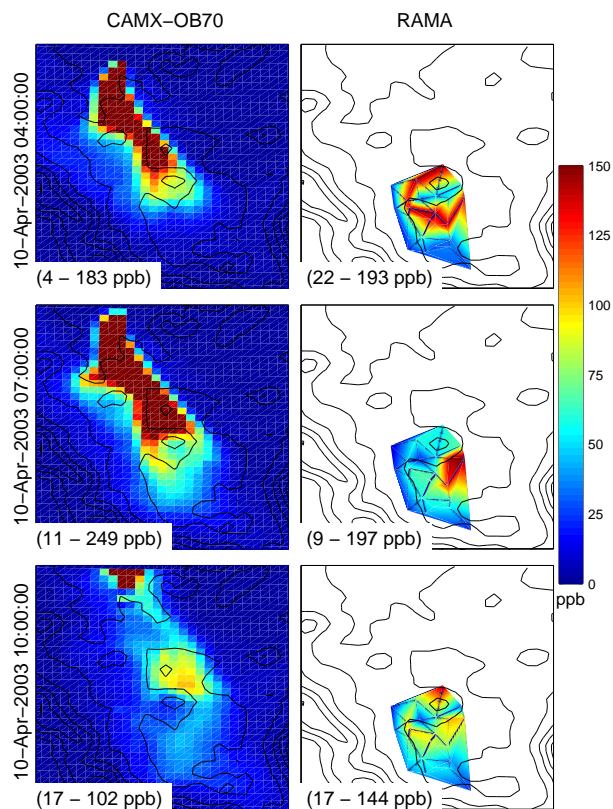


Fig. 17. Surface concentration of SO₂ from model (left) and RAMA observations (right) at 04:00, 07:00 and 10:00 CDT during the SO₂ plume episode of 10 April 2003. Numbers in brackets show the domain-wide minimum and maximum concentrations of the measurements for the RAMA plots, and of the model area corresponding to the measurement locations for the CAMx plots.

[Title Page](#)[Abstract](#)[Introduction](#)[Conclusions](#)[References](#)[Tables](#)[Figures](#)[◀](#)[▶](#)[◀](#)[▶](#)[Back](#)[Close](#)[Full Screen / Esc](#)[Printer-friendly Version](#)[Interactive Discussion](#)

Sources and transport of CO and SO₂ in the MCMA

B. de Foy et al.

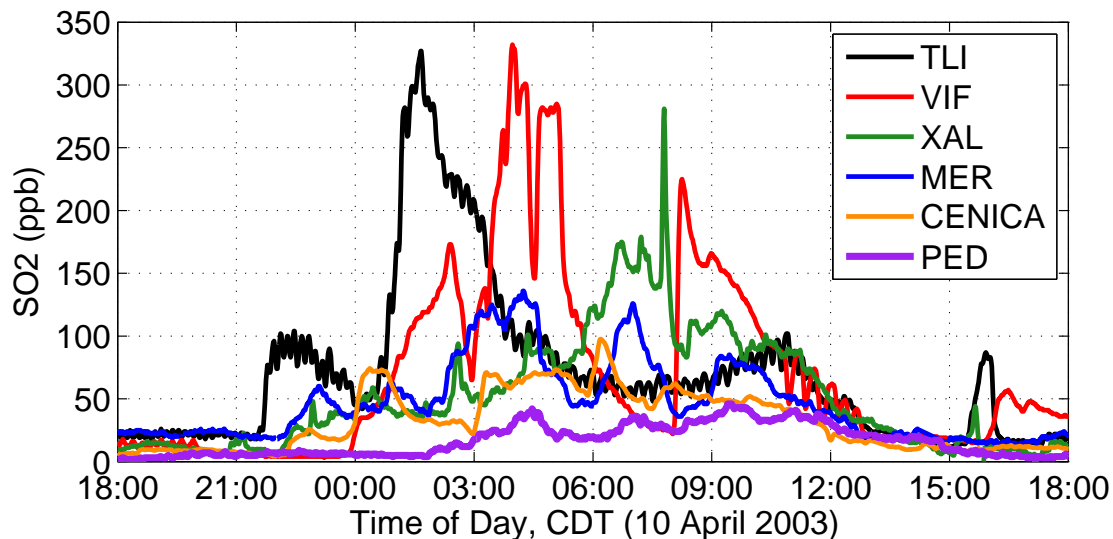


Fig. 18. Time series of measured SO₂ concentrations at 1-min resolution for 10 April plume event at selected RAMA stations and at CENICA.

[Title Page](#)[Abstract](#)[Introduction](#)[Conclusions](#)[References](#)[Tables](#)[Figures](#)[◀](#)[▶](#)[◀](#)[▶](#)[Back](#)[Close](#)[Full Screen / Esc](#)[Printer-friendly Version](#)[Interactive Discussion](#)